PB80-221930

Aerosol Size Measurement by Electrical Mobility and Diffusion Analysis A Comparison of Methods

Paris-6 Univ. (France)

Prepared for

Environmental Sciences Research Lab.
Research Triangle Park, NC

Sep 80

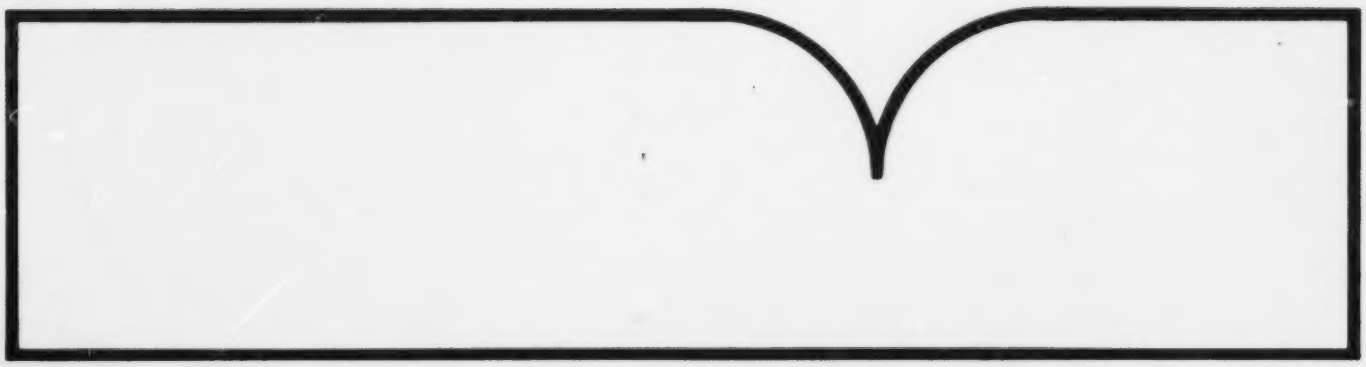

U.S. Department of Commerce
National Technical Information Service
NTIS

TYPING GUIDE SHEET
BEGIN FIRST LINE OF TEXT HERE
CENTER OF PAGE
TOP OF IMAGE AREA

PB80-221930

EPA-600/3-80-088
September 1980

AEROSOL SIZE MEASUREMENT BY ELECTRICAL MOBILITY AND DIFFUSION ANALYSIS

A Comparison of Methods

by

J. Bricard

University of Paris
Paris, France

and

G. Madelaine and M. L. Perrin

Office of Atomic Energy
Fontenay-aux-Roses, France

Grant 804370

Project Officer

T. G. Ellestad
Atmospheric Chemistry and Physics Division
Environmental Sciences Research Laboratory
Research Triangle Park, North Carolina 27711

REPRODUCED BY
NATIONAL TECHNICAL
INFORMATION SERVICE
U.S. DEPARTMENT OF COMMERCE
SPRINGFIELD, VA 22161

ENVIRONMENTAL SCIENCES RESEARCH LABORATORY
OFFICE OF RESEARCH AND DEVELOPMENT
U.S. ENVIRONMENTAL PROTECTION AGENCY
RESEARCH TRIANGLE PARK, NORTH CAROLINA 27711

BEGIN LAST LINE OF TEXT
BOTTOM OF IMAGE AREA, OUTSIDE DIMENSION FOR TABLES AND ILLUSTRATIONS
3/8"
PAGE NUMBER
EPA-287 (Cin.)
(4-76)

TECHNICAL REPORT DATA
(Please read Instructions on the reverse before completing)

1. REPORT NO.	2.	3. RECIPIENT'S ACCESSION NO.
EPA-600/3-80-088		PB80 221930

4. TITLE AND SUBTITLE	5. REPORT DATE
AEROSOL SIZE MEASUREMENT BY ELECTRICAL MOBILITY AND DIFFUSION ANALYSIS A Comparison of Methods	Sept. 1980 Issuing Date. 6. PERFORMING ORGANIZATION CODE
7. AUTHOR(S) J. Bricard, G. Madelaine and M.L. Perrin	8. PERFORMING ORGANIZATION REPORT NO.
9. PERFORMING ORGANIZATION NAME AND ADDRESS University of Paris Paris, France	10. PROGRAM ELEMENT NO. C07A1D/01-0433 (FY-80) 11. CONTRACT/GRANT NO. 804370
12. SPONSORING AGENCY NAME AND ADDRESS Environmental Sciences Research Laboratory - RTP, NC Office of Research and Development U.S. Environmental Protection Agency Research Triangle Park, North Carolina 27711	13. TYPE OF REPORT AND PERIOD COVERED Final 9/76 - 9/79 14. SPONSORING AGENCY CODE EPA/600/09

15. SUPPLEMENTARY NOTES

16. ABSTRACT

The principle of the electrical aerosol analyzer method is reviewed and the diffusion battery method is described in detail. An appendix explains the basis of the calculations used. The diffusion battery method is complicated by counting losses of very small particles, inherent to condensation nuclei counters. A calibration of such counters is described, and results are introduced into the diffusion battery method; the mathematical details of this correction are discussed in a second appendix. Thus, the real size distribution of a polydisperse, ultrafine aerosol is obtained.

The experimental use of the diffusion battery method is described for a monodisperse aerosol produced by radiolysis of gaseous impurities of air, and the smallest particle diameter detectable with this method is determined. The two methods are compared for aerosols produced by radiolysis and photolysis of gaseous impurities of air; they are in good agreement only for particles larger than 0.01-0.02 μm diameter. The electrical aerosol analyzer gives no useful data for smaller particles. The two methods are compared using an experimental device modified for atmospheric aerosol measurement. These results confirm laboratory results; we obtain a good agreement between the two methods for particles with diameter greater than 0.01 μm, and no measurements with the electrical aerosol analyzer are possible for smaller particles.

17. KEY WORDS AND DOCUMENT ANALYSIS

a. DESCRIPTORS	b. IDENTIFIERS/OPEN ENDED TERMS	c. COSATI Field/Group
Air pollution *Aerosols Particle size distribution Reviews	Electrical aerosol analyzer method Diffusion battery method	13B 07D 05B

18. DISTRIBUTION STATEMENT	19. SECURITY CLASS *(This Report)*	21. NO. OF PAGES
RELEASE TO PUBLIC	UNCLASSIFIED	79
	20. SECURITY CLASS *(This page)*	22. PRICE
	UNCLASSIFIED	

DISCLAIMER

This report has been reviewed by the Environmental Sciences Research Laboratory, U.S. Environmental Protection Agency, and approved for publication. Approval does not signify that the contents necessarily reflect the views and policies of the U.S. Environmental Protection Agency, nor does mention of trade names or commercial products constitute endorsement or recommendation for use.

BEGIN FIRST LINE OF TEXT HERE
TYPING GUIDE SHEET
CENTER OF PAGE
TOP OF IMAGE AREA
DROPPED HEAD: BEGIN SECTIONS HERE

ABSTRACT

The principle of the electrical aerosol analyzer method is reviewed briefly, and the diffusion battery method is described in detail, with emphasis on the physical basis of the method. An appendix explains the basis of the calculations used and is an aid in obtaining valuable results from the physical measurements. The diffusion battery method is complicated by counting losses, especially of very small particles, inherent to condensation nuclei counters. A calibration of such counters is described, and results are introduced in the above-mentioned results obtained with the diffusion battery method; the mathematical details of this correction are discussed in a second appendix. With this method, the real size distribution of a polydisperse, ultrafine aerosol is obtained.

The experimental use of the diffusion battery method is described for a monodisperse aerosol produced by radiolysis of gaseous impurities of air, and the smallest particle diameter detectable with this method is determined. The two methods are compared for aerosols produced by radiolysis and photolysis of gaseous impurities of air; they are in good agreement only for particles larger than 0.01-0.02 μm diameter. The electrical aerosol analyzer gives no useful data for smaller particles. The two methods are compared using an experimental device modified for atmospheric aerosol measurement. The results of the comparison confirm laboratory results; we obtain a good agreement between the two methods for particles with diameter greater than 0.01 μm, and no measurements with the electrical aerosol analyzer are possible for smaller particles.

This report was submitted in fulfillment of Grant No. 804370 by the University of Paris under the partial sponsorship of the U.S. Environmental

BEGIN LAST LINE OF TEXT HERE
BOTTOM OF IMAGE AREA, OUTSIDE DIMENSION FOR TABLES AND ILLUSTRATIONS
3/8"
FOOTER MARGIN
PAGE NUMBER
EPA-267 (Cin.) (4-76)

Protection Agency. This report covers the period September 15, 1976, to September 14, 1979, and work was completed as of October 3, 1979.

CONTENTS

Abstract. iii
Figures vi

1. Introduction. 1
2. Conclusions 2
3. Systems Description and Operative Principles. 3
    Electrical aerosol analyzer 3
    Diffusion battery 6
4. Experimental Results. 16
    Preliminary experimentation with artificial aerosol 16
    Comparison with natural aerosol 25

References. 42
Appendices

A. Algorithm to Solve System of N Equations. 43
B. Introduction of Counting Losses in the Maigne Method. 65

FIGURES

Number		Page
1	Schematic system diagram of the EAA.	28
2	Variation in $\bar{n}/n_o$ ratio as a function of flow rate	29
3	Aerosol generator.	30
4	Variation in N_c/N_a ratio for varying diameter size	31
5	Experimental device for radiolysis experiment.	32
6	Variation in "apparent" particle number as a function of time, according to DBM measurements	33
7	Variation in time of particle size, according to CNC measurements, and corrected for counting losses.	33
8	Variation as a function of time in "apparent" radius produced by radiolysis, for different values of n_{max}	34
9	Evolution with time of "apparent" total particle concentration, as indicated by CNC.	34
10	Size distribution obtained by DBM at two different times	35
11	Size distributions obtained by DBM and EAA after 4 h	35
12	Size distributions obtained by DBM and EAA after 2 h	35
13	Bimodal size distributions obtained by DBM and EAA	35
14	Calculated v. measured attenuation at each battery stage for four diameter sizes.	36
15	Evolution of real number/size distribution obtained by DBM	37
16	Variation as a function of time in number, surface, and volume, measured by DBM.	37
17	Number/size distribution 1 h after irradiation, measured by EAA and DBM.	38
18	Number/size distribution 3 h after irradiation, measured by EAA and DBM.	38
19	Concentration as a function of time.	39
20	Volume as a function of time	39
21	Surface area as a function of time	39

Number		Page
22	Percent of particles penetrating to each of the 11 stages at 3 different times of day	40
23	Variation with time in the number/size distribution of natural aerosol.	40
24	Comparison of number/size distribution measurements with EAA and DBM at 7:30 am	41
25	Comparison of number/size distribution measurements with EAA and DBM at 9:00 am	41
26	Concentration as a function of time, corrected for counting losses, as indicated by DBM.	41
1A	. . . . .	50
2A	. . . . .	50
3A	. . . . .	51
4A	. . . . .	51
5A	Fortran program.	52

SECTION 1

INTRODUCTION

Two different in-situ techniques are currently used to establish the size distribution of Aitken nuclei, or particles with diameter (d) < 0.2 μm. These techniques are the electrical aerosol analyzer (EAA) method and the diffusion battery method (DBM).

The present study is a comparison of experimental results obtained with the two methods. A brief review is presented for the principle of the EAA method, the basis for commercially available equipment. A detailed description of the DBM technique and supporting calculations are given. Laboratory results are obtained using the two techniques to measure artificially-produced aerosol, and these results are compared with values obtained in measuring natural aerosol.

SECTION 2

CONCLUSIONS

Results of two preliminary laboratory experiments were similar. Aerosols of very small particles were produced artificially from gaseous impurities of air, first by radiolysis, and in a second experiment by photolysis. In radiolyzed aerosol, for particles with $d < 0.01$ μm, the DBM permitted a good estimate of particle size distribution, while the EAA data were useless; for aerosol particles with $d > 0.02$ μm, the methods were in agreement. For photolytic particles with $d > 0.01$ μm, comparable results were produced by the DBM and EAA measurement methods; in addition, the DBM allowed detection of the ultrasmall portion of the size distribution range (0.002 to 0.01 μm). This ultrasmall portion must be studied in analyzing homogeneous and heterogeneous nucleation — processes which, together with coagulation, govern the evolution of fine particles.

Natural aerosol was measured near the laboratory at Fontenay-aux-Roses, producing results predictable from the preliminary laboratory experiments. Numerous comparisons were made between the two methods for atmospheric particles, resulting in good agreement for particles in the range of $d = 0.01$ to 0.1 μm. For particles where 0.002 μm $< d < 0.01$ μm, only the DBM appeared to provide useful data.

SECTION 3

SYSTEMS DESCRIPTION AND OPERATIVE PRINCIPLES

ELECTRICAL AEROSOL ANALYZER

Instrumentation and Method

The EAA instrument shown schematically in Figure 1 consists of three major parts: the aerosol charger, the particle precipitator, and the electrometer sensor, together with associated electronics and flow controls (1). The instrument samples aerosol at the rate of 4 liters/min. An additional 46 liters/min of air is necessary for the mobility analyzer, making a total air requirement of 50 liters/min for the instrument system. As Figure 1 shows, aerosol is first sampled into the charger to expose all the particles to unipolar positive ions produced by a corona discharge. The charged aerosol then enters the mobility analyzer, comprising the precipitator and the electrometer sensor. The mobility distribution is then measured, and from this measurement the particle size distribution is inferred. The manufacturer notes that EAA values for particles with $d < 0.01$ μm are not valid, except in the case of a perfectly monodisperse aerosol.

The precipitator and electrometer sensor together function as a mobility analyzer. The precipitator is in the form of a flow condenser with concentric cylindrical electrodes. The collector rod is held on insulating supports and centered in the tube. The outer tube is grounded, while the potential on the collecting rod can be varied from 0 to -10.6 kV.

The charged aerosol is introduced into the precipitator through a side opening on the tube and flows down the precipitating region in the form of an

annular sheath around a core of particle-free clean air. In the precipitator, the charged particles are deflected by the electric field toward the collector rod. Particles with sufficiently high mobility are precipitated; those with lower mobilities escape collection by the precipitator, are detected by the electrometer sensor, and are removed from the air stream by an absolute filter in the sensor. The critical cutoff mobility, Z_p, when precipitation occurs, is given by:

$$Z_p = \frac{Q_t \log_e (R_2/R_1)}{2 \pi V L} \qquad (1)$$

where Q_t = total inflow rate in the mobility analyzer
R_1 = inner radius of precipitator electrode
R_2 = outer radius of precipitator electrode
L = length of collector rod
V = voltage of collector rod

The relationship between the particle mobility and operating parameters of the precipitator given by Equation 1 is exact, irrespective of the flow rate in the precipitator.

Measurement of the complete distribution consists of stepping through a given sequence of voltages of the collecting rod and recording the corresponding electrometer current, I, at each voltage step. All measurements can be completed in about 2 min. A table accompanying the EAA shows the standardized operational and calculation steps necessary to obtain the size distribution of the particles. The particle diameter range has been divided into geometrical increments of four/decade, or a total of ten geometrical size intervals from 0.0032 μm to 1 μm.

In the above table, the difference in electrometer current from step to step is multiplied by a constant, $\Delta N/\Delta I$, to obtain the particle concentration within that size interval. The multiplying constant is calculated from the equation:

$$\Delta I = \Delta N \, Q \, n_p \, e \, f_e \, f_p \qquad \text{Amp} \qquad (2)$$

where Q = sample flow rate in the charger (66.7 cm^3/sec, or 4 liters/min)

n_p = mean particle charge (elementary units)

e = elementary charge (1.609 x 10^{-19} coulombs)

f_e = fraction of particles in each size interval that is electrically charged and therefore precipitated

f_p = fraction of particles in each size interval that penetrates the system and is collected by the electrometer current sensor.

The calibration constants, f_e and f_p, for each size interval have been obtained by the procedure described by Whitby and Liu (2). A moderately monodisperse aerosol of suitable size was first generated, and the particle concentration upstream of the charger and downstream of the generator was measured with a condensation nuclei counter (CNC). The fraction of particles lost in the charger, precipitator, and flow tubing is $1 - f_p$.

Principle

To measure the size distribution of an aerosol from its electrical mobility, the functional relationship between mobility and particle size must be monotonic. As Whitby and Clark (3) first pointed out, the electrical mobility of an aerosol charged under conditions closely approximating that of diffusion charging is a monotonically decreasing function of the particle size for particles with diameter smaller than ~1 μm. Thus, the diffusion charging mobility analysis principle can be the basis of a size distribution measuring principle for submicron aerosols.

The theoretical calculations of Bademosi (4), relating the electrical mobility and the particle size for diffusion charging, have been applied for several different values of the charging parameter $N_o t$, where N_o is the ion concentration and t the charging time; these calculations have also been applied to the relationship between particle charge and particle size. Since

a finite slope in the "mobility particle size" curve is needed for size determination, the method has an upper size limit of ~1 μm. Further, the slope of the curve becomes steeper when the $N_o t$ value is reduced. Thus, for size discrimination, small values of $N_o t$ are preferred.

The requirement of a small $N_o t$ value near the upper size limit of the instrument is in opposition to the value requirement near the lower size limit, where the instrument sensitivity for detecting small particles depends on the particle fraction that is electrically charged; consequently, instrument sensitivity is higher in the latter case. Thus, the actual instrument design is a necessary compromise between these opposite requirements. In the actual instrument, an $N_o t$ value of 1×10^7 sec/cm^3 has been chosen. For that value and particle diameters smaller than ~0.02 μm, the mean charge on the particles becomes less than one elementary unit. In this region, only a fraction of the particles is electrically charged; the fraction consists essentially of particles carrying one elementary unit of charge. The sensitivity of the device in this region would therefore be questionable.

DIFFUSION BATTERY

Principle

A diffusion battery is a cluster of parallel, equidistant plates or a cluster of parallel, rectilinear identical tubes. Currently, the DBM system presents the best method for establishing the size distribution for aerosols of very small particles ($d < 0.1$ μm), because it theoretically permits access to molecular dimensions. Moreover, in contrast with the electron microscope, the DBM does not modify the particles under study.

In the DBM system, an aerosol passes through the diffusion battery. Let n_o represent the mean concentration of the upstream particles, and $\bar{n}$ the mean concentration of the downstream particles. Passage through the battery results in aerosol losses to the walls of the tubes (flat or cylindrical) by Brownian movement of the particles and by diffusion. The value of the fraction $\bar{n}/n_o$ is dependent on the size distribution of the aerosol.

Monodisperse Aerosol —

The following hypotheses are assumed: the air flow is laminar, every particle striking the walls is trapped, and particle removal results only from Brownian diffusion.

Let $\mu = \alpha D$, and D = diffusion coefficient of the particles. In the case of cylindrical canals of total length L:

$$\alpha = \frac{\pi L}{Q} \tag{3}$$

where Q = flow rate of air through each individual canal.

In the case of a flat canal battery:

$$\alpha = \frac{2 bL}{aQ} \tag{4}$$

where b = width of each flat canal

a = one-half the depth of each flat canal

Calculations of Gormley and Kennedy (5), Marcus and Thomas (6), and Thomas (7) give $\bar{n}/n_o$ for two cases. For $\mu < 0.01$,

$$\frac{\bar{n}}{n_o} = 1 - A\,\mu^{2/3} + B\,\mu + C\,\mu^{4/3} \tag{5}$$

For $\mu > 0.01$,

$$\frac{\bar{n}}{n_o} = \sum_i a_i \exp(-b_i \mu) \tag{6}$$

For cylindrical batteries

A = 2.56	B = 1.2	C = 0.177
a_1 = 0.8190	a_2 = 0.0972	a_3 = 0.0325
b_1 = 3.6968	b_2 = 22.305	b_3 = 56.95

and for flat canal batteries

$A = 1.175$	$B = 0.1$	$C = 0.0175$
$a_1 = 0.909$	$a_2 = 0.053$	$a_3 \approx 0$
$b_1 = 1.885$	$b_2 = 21.43$	$b_3 = 0$

when $\bar{n}/n_o$ has been measured for the given battery and flow rate. The corresponding D characterizing the aerosol is determined from the above relations. The corresponding particle radius is given from the Millikan formula:

$$D = \frac{kT}{6 \pi R \eta} \left[1 + A \frac{l}{R} + B \frac{l}{R} \exp -C \frac{R}{l} \right] \qquad (7)$$

where T = temperature (degrees Kelvin)

k = Boltzman constant (1.38×10^{-16} dyne x cm/deg)

l = mean free path of the air molecules

A = 1.246

B = 0.42

C = 0.87

R = particle radius

η = viscosity (1.8×10^{-4} g/cm/sec)

Polydisperse Aerosol —

To apply the DBM to a polydisperse aerosol, the Twomey method (8) is used. For a given battery and flow rate (i.e. for a given value of parameter α), $\bar{n}/n_o$ depends on D (or on the particle dimensions) as shown in Equation 6.

Let f(D) be the diffusion coefficient distribution of the aerosol in transit. The aerosol is characterized by a concentration n_o f(D) dD with a diffusion coefficient between D and dD. For a polydisperse aerosol, it can be shown that:

$$\frac{\bar{n}}{n_o} = \frac{1}{n_o} \int_0^\infty f(D) \rho (D,\alpha) dD \qquad (8)$$

In Equation 8, ρ (D,α) is the particle fraction, with diffusion coefficient D, which for a given value of α (or for a given battery, for a given flow rate) is transmitted by the battery. According to the above relations:

$$\rho\ (D,\alpha) = \sum_i a_i \exp\ (-b\ \alpha\ D) \qquad (9)$$

Determining f(D) from the Fredholm relation of Equation 8 presents a problem. It can be shown that this may have an exact solution only if the first member has an analytical form; in other words, if $\bar{n}/n_o$ is known with very great precision, which is impossible to achieve experimentally. A major difficulty is therefore recognized in determining the size distribution function of polydisperse aerosols by the DBM.

Maigne Method —

The f(D) of the aerosol to be studied is supposed in the form of a classical histogram comprising N different classes. Let D_1 represent the smallest diffusion coefficient, and let us suppose that D_1 is known. That is the only hypothesis, which will be justified later. A series of intervals is defined:

$$D_1D_2,\ D_2D_3,\ \ldots\ D_iD_{i+1}\ \ldots\ D_ND_{N+1} \qquad (D_{i+1} > D_i \text{ for } i = 1, N)$$

We associate to the value D_{i+1} the corresponding values α_i given by the relations seen in Equations 3 and 4. This series of values α_i corresponds to either a series of flow rate values for a given battery, or a series of successive lengths L_1 .... L_i of the battery for a given flow rate; and for each pair of values — D_{i+1}, Q_i or D_{i+1} — the function $\bar{n}/n_o$ (D, Q) or $\bar{n}/n_o$ (D, 1) $\approx$ 0.01. This means nearly all particles with diffusion coefficient $> D_{i+1}$ are trapped by the battery under these conditions.

If the fraction $\bar{n}_i/n_o$ represents the ratio of the mean concentration after versus before the battery, in conditions characterized by the value α_i, one can write:

$$\frac{\bar{n}_i}{n_o} = \frac{\int_{D_1}^{D_{i+1}} f(D)\ \rho\ (D, \alpha_i)\ dD}{n_o} \qquad \text{for } i = 1 \ldots N \qquad (10)$$

where ρ is given by Equation 9. In every case, μ is assumed greater than 0.01.

When intervals $D_i\ D_{i+1}$ are sufficiently small, f(D) can be considered as a constant along each of them. The size distribution spectrum can be represented by a classical histogram. One can write:

$$\frac{\bar{n}_i}{n_o} = \frac{1}{n_o}\ Y_1 \int_{D_1}^{D_2} \rho(D, \alpha_1)\ dD + \ldots\ Y_i \int_{D_i}^{D_{i+1}} \rho\ (D, \alpha_i)\ dD \qquad (11)$$

Let

$$X_{ij} = \int_{D_j}^{D_{j+1}} \rho\ (D, \alpha_i)\ dD \qquad (12)$$

therefore

$$\frac{\bar{n}_i}{n_o} = \sum_{j=1}^{1} X_{ij}\ Y_j\ \frac{1}{n_o} \qquad i = 1 \ldots N \qquad (13)$$

The components of the vector $\bar{n}/n_o$ are the experimental values of $\bar{n}/n_o$ for the different values of α_i, X_{ij}, defined by Equation 12, and are calculated from Equation 13 by the following method.

For a polydisperse aerosol, as previously stated, the smallest diffusion coefficient D_1 must be determined by a method other than the DBM. Thus, an approximation is made to f(D), which becomes more satisfactory as the number of elements is increased.

Let us suppose N measurements of $\bar{n}/n_o$ are made before and after the diffusion battery. That corresponds to a linear system of N equations with N unknowns, as represented by Equation 13. Obtaining an exact solution for this system would be valuable, but physically impossible because of the poor precision characterizing the experimental values of $\bar{n}/n_o$.

A linear solution is attempted by introducing limits on f(D). For that, Maigne (9) and Maigne et al. (10) redistribute the N classes of D into M classes, with $M < N$, each of these new classes comprising several successive segments; and along each segment, f(D) is assumed lognormal. The size distribution is determined by M successive and contiguous elements within M lognormal distributions that are different.

The smallest diffusion coefficient (or, equivalently, the largest diameter) is known because of the continuity conditions between the successive elements of the lognormal distribution. Therefore, the system of Equation 13 is replaced by a system of N equations with M independent variables, which are the mean geometrical diameters of the M lognormal distributions. The distributions of the M segments are approximately equal to the real distribution of the real aerosol.

A valuable solution of the equations is given by an algorithm, presented in Appendix A, and based on the following considerations:

- Account for M equations only, conveniently chosen from the N equations proposed
- Determine D_1 by successive approximations
- Account for experimental error in $\bar{n}/n_o$ measurements corresponding to different flow rates (or different lengths of circular tubes).

In practice, the experimental measurements are processed using a Fortran program (Appendix A, Figure 5A). Data input for a flat canals battery includes:

- diffusion unit dimensions: plate length and width, number of plates, and half-distance between the plates
- D_1
- a series of diffusion coefficients defining a series of diameter classes
- the $\bar{n}/n_o$ ratios from measurements taken of condensation nuclei upstream and downstream, respectively, from the diffusion unit.

The computer provides percentages of particles according to diameter class. With this method, therefore, the particle size distribution of an aerosol can be determined when the mean concentration measurements are known upstream and downstream of the diffusion unit, i.e., n_o and $\bar{n}$, at a given time for various flow rates through the diffusion unit.

Figure 2 shows the experimental curve $\bar{n}/n_o$ for different values of flow rate for a flat canals battery (the curve has been smoothed from 8 measurement points) and the same calculated again from the algorithm.

Counting of the Particles

Principle —

The mean concentrations, n_o and $\bar{n}$, before and after the battery (or each length of the battery, as will be seen later) are measured with a CNC manufactured by General Electric. This counter consists of an expansion chamber where saturated air, containing particles, is introduced. Expansion produces a cooling of the saturated air, and a supersaturation of about 400 percent. Each particle yields a droplet, and the droplets (and, consequently, the particles) are counted by measurement of light scattered by the droplets.

The supersaturation of 400 percent corresponds to a depression of 20 cm Hg; since this depression is slightly greater than the depression corresponding to homogeneous nucleation, the condition exists for teh best counting efficiency. Each measurement has a duration of 0.2 sec.

Let p be the water vapor pressure in the expansion chamber, and p_∞ the saturated pressure at the temperature T in degrees Kelvin. According to the Kelvin relation:

$$\log_e \left(\frac{p}{p_\infty}\right) = \frac{2\,\sigma\,M}{\rho\,R_g\,TR} \qquad (14)$$

where ρ = density of the liquid droplet

M = molar mass of the liquid droplet

σ = surface tension

R_g = gas constant

R = radius of the droplet in equilibrium at these conditions.

According to Equation 14 — in the case of water, perfect wetting of the nuclei, and p/p_∞ = 400 percent — condensation on the nuclei (formation of droplets) is possible only if particle d > 0.0014 μm.

Calibration of the Counter —

We have used a generator of monodisperse aerosols described by Liu and Pui (11); this unit is briefly described.

A polydisperse aerosol is produced by atomizing the solution of a given salt; the aerosol is then dehydrated and electrically charged by a system similar to that of the EAA. A cylindrical condenser containing an electric field (E) allows trapping of a monodisperse aerosol at distance L from the entrance by means of an axial hollow electrode (Figure 3). The concentration N_a (particle number/cm^3 air) is known from the electrical charge of the aerosol issuing from the tube, which is measured with an electrometer. By varying E, one can obtain an aerosol of given mobility, and consequently a monodisperse aerosol with particles of a given diameter (2 R = d).

This aerosol is introduced into the CNC. Let N_c be the concentration indicated by the counter, according to manufacturer specifications. Our measurements (12), in agreement with Liu and Kim (13), indicate N_c is generally smaller than N_a; variations in N_c/N_a for different diameters are shown in

Figure 4, corresponding to aerosols of various constituents (NaCl, Na_2SO_4, H_2SO_4). In every case, N_c/N_a diminishes with decreasing diameter. N_c/N_a is about equal to unity for $d > 0.05$ μm and decreases to 0.06 for $d = 0.004$ μm. Because of the uncertainty of the measurements, it is not possible to precisely estimate the influence of the particle composition.

In our measurements, mean values are assumed. Later, the smallest diameter which can be detected with the CNC is discussed.

The particles issuing from the monodisperse aerosol are electrically charged, and the possible effect of this electrical charge caused concern. We therefore neutralized this electrical charge by using a radioactive source (tritium, 200 mc) located within a cylindrical tube through which the aerosol passes (14). Following neutralization, sufficiently small ($d < 0.01$ μm) particles were verified to have no detectable electric charge. For particle concentrations between 50,000 to 80,000/cm^3, no appreciable difference in concentration measurements by the CNC was detected, either with or without neutralization.

Currently, no satisfactory explanation for counting losses in the CNC is offered. Nevertheless, a corresponding modification of the results, given directly by the Maigne method, is introduced.

With the Maigne method, f(D), representing the diffusion coefficient distribution, was determined with no allowance for counting loss. Let $\Psi_1(d)$ be the uncorrected size distribution function; $d = 2R$ = diameter of the particles corresponding to f(D) and given by Equation 7. Of course, $\Psi_1(d)$ is a hypothetical function.

Let $\Phi(d) = N_c/N_a$, the experimental counting losses corresponding to the diameter d. It can be shown (Appendix B) that the true size distribution function is given by the relation:

$$\Psi(d) = \frac{1}{\Phi(d)} \Psi_1(d) \qquad (15)$$

and the total counting concentration will be:

$$N = \int_0^\infty \frac{1}{\Phi(d)} \Psi(d)\, dd \qquad (16)$$

For an aerosol characterized by a histogram of interval Δd_i,

$$N = \sum_i \frac{\Delta n_i}{\Delta d_i} \frac{1}{\Phi(d_i)} \qquad (17)$$

SECTION 4

EXPERIMENTAL RESULTS

In a preliminary experiment, the EAA and DBM measurement methods were compared using an aerosol of very small particles. The aerosol was artificially produced by radiolysis or photolysis of gaseous impurities in atmospheric air. Data from this preliminary work were used to refine the methodology in a subsequent experiment, which was a quantitative comparison of results provided by the two methods for determining experimental size distribution of an atmospheric aerosol.

PRELIMINARY EXPERIMENTATION WITH ARTIFICIAL AEROSOL

Radiolysis Aerosol

Experimental Device —

The main circulation system (Figure 5) contains a spherical, acrylic plastic enclosure (1) with an 800-liter capacity. The sphere is kept in darkness (to avoid simultaneous photolysis) and preceded by two series-mounted dihedral filters. Aerosol production is begun by circulating air over actinium (Ac^{227}), which produces the radioactive gas, actinon (also called radon-219). The actinon gas, with a very short half-life (3.9 sec), is filtered and then transported by the air current into the plastic sphere. A rotameter is used to measure the flow rate of the air current. A fan, preceded by an absolute filter to prevent escape of radioactive particles, discharges the current to the exterior.

Pressure in the sphere is controlled by a pressure gauge mounted on the enclosure. A safety device, comprising a valve and a filter, discharges

excess aerosol to the atmosphere to avoid overpressure while the radioactive gas is injected into the sphere. The enclosure is incapable of sustaining a positive or negative pressure that exceeds 250 mm Hg.

A diffusion battery with 10- by 35-cm rectangular plates separated by a 0.24-cm half distance is used. The airflow rate through the unit is adjusted by a system comprising a rotameter, a fan, and a vent to the atmosphere. The unit is equipped with two sampling circuits — one upstream, one downstream of the battery — connected to the actual measuring device by a single path. The arrangement allows separate sampling upstream and downstream of the unit. The particle concentration is measured with a CNC.

Preliminary Experiments —

Filtered, atmospheric air is circulated through dihedral filters and through the enclosure until the CNC indicates a value on the order of its minimum detectable concentration. At this point, the enclosure contains only the natural air and its gaseous impurities. Actinon from the previously described device is then injected into the enclosure to disintegrate and thereby produce radiolysis of the gaseous impurities present. The radioactive gas is injected for a short period (on the order of 2 min) and at a constant rate. Since the half-life of actinon is very short, particle production is considered instantaneous. Once injection is complete, the particles are allowed to move around, and concentrations are measured upstream and downstream of the diffusion unit.

Approximately 90 min after the actinon is injected, a second injection of the radioactive gas is introduced into the enclosure, under the original conditions, to produce a second aerosol of ultrasmall particles. Concentrations upstream and downstream of the unit are again measured at a given time and for various flow rates through the unit.

Figures 6 and 7 show results of these experiments. Figure 6 represents the evolution in time of the total "apparent" concentrations of particles measured upstream of the system using the DBM method. Apparent measurements are values that do not introduce counting loss corrections.

After the first injection of actinon, the concentration quickly increases as a function of time until it reaches a maximum value, $n_{1\ max}$, at time, $t_{1\ max}$, beginning with the entry of the radioactive gas into the sphere. Following $t_{1\ max}$, the concentration decreases. As soon as the second quantity of radioactive gas is injected, the concentration again quickly increases to a second maximum value, $n_{2\ max}$, at the time, $t_{2\ max}$, after which the concentration decreases. Maximum values are reached ~10 min after the radioactive gas is injected into the sampling sphere. Time t_1 represents the instant at which the particles are in equilibrium and starts from the beginning of the first injection of actinon; t_2 represents the instant at which they are in equilibrium, starting from the beginning of the second injection.

Figure 7 represents the evolution in time of the particle size, obtained from direct indications of the counter, and corrected for counting losses introduced by Equation 15. The particle size is observed to be unimodal 20 min and 90 min after the injection of radioactive gas. It has a maximum value which moves with time toward increasing radii, the amplitude of this value decreasing with time. The number of larger particles increases as the number of the smaller ones decreases, a result of the coagulation phenomenon.

Five minutes after the second injection of actinon, the particle size becomes bimodal. The first mode reflects the ultrafine particles created through radiolysis; the second mode represents the particles remaining from the first actinon injection. Then 25 min following the second injection of radioactive gas, the particle size again becomes unimodal, because second-injection small particles coagulate with the large particles already present. The number of small particles decreases quickly, while the number of large particles rapidly increases, until the first mode disappears.

During this radiolysis experiment, a sample was taken upstream of the diffusion battery as the radioactive gas was introduced. No deviation of the CNC needle was observed during a "lapse time," T, of 45 to 50 sec following introduction of the gas. This lapse time, T, is the time necessary for the particle radius to evolve from the critical radius, r_c, to the minimum

detectable value, r_d, for the CNC. The particle radius r_c is assumed to be instantaneously reached.

Let us suppose, as a first approximation, that the aerosol is monodisperse before the second injection. With Equations (6) and (7) and measurements of $\bar{n}/n_o$ upstream and downstream of the diffusion battery, variations of the mean apparent radius can be deduced as a function of time for different values of n_{max} (depending on the quantity of actinon introduced and on the concentration of gaseous impurities in the sphere).

The r_d location on the graph in Figure 8 is at t = 45 to 50 sec; during this time, no deviation of the CNC needle was seen. In our experiments, the sensitivity threshold was found at d = 17 to 18 Å. These results are based on definite conditions (e.g., water vapor), and any modification of these conditions yields a change in values. Generally speaking, the value limits are between 16 and 24 Å.

The r_c of radiolytic particles is the minimum radius that will allow particle stability and development by condensation of the supersaturated gases present. This r_c can be obtained by extrapolating the curves (Figure 8) at time t, defined as the time when the r_c is attained. Time t cannot be determined experimentally, but it is assumed very close to the time when the radioactive gas was first injected. For practical reasons, extrapolation was made at t = 10 sec, counted from the start of the actinon injection.

Depending on the concentration of gaseous impurities in atmospheric air and on humidity, r_c decreases as nucleation frequency (i.e., n_{max}) increases. As seen in Figure 8, and accounting for experimental conditions, r_c was between 5 and 7.5 Å, in good agreement with nucleation theory (15,16).

Comparison Between EAA and DBM with the Radiolysis Aerosol —

The methods comparison is carried out during a series of three experiments. In the first one, a low particle production (<50,000/cm^3) is observed. In the second one, particle production is high, and the n_{max} detected by the

CNC is greater than 2 x $10^6/cm^3$. In the third experiment, radioactive gas is again injected into the vessel, under the original conditions, in order to create an aerosol of very small particles.

Experiment 1: low production of particles — The curve in Figure 9 represents the qualitative evolution with time, without account for counting losses, of the total particle concentration directly indicated by the CNC. A low particle production is therefore reflected in this case, and $n_{max} < 50{,}000/cm^3$. Figure 10 shows the evolution of the size distribution obtained by DBM given directly by the Maigne method. Curves show a maximum that shifts in time toward increasing radii.

A size distribution of the given aerosol cannot be measured with the EAA. Figure 10 shows that d = 0.001 to 0.01 μm after about 2 h, and evolves very little afterwards, because of the low production level at the start of these experiments. The dimensions correspond to the first two EAA channels, which lack the sensitivity for detecting particles in this size range.

Experiment 2: high production of particles — During a second experiment, a stronger irradiation of filtered atmospheric air yielded a high production of particles. In this case, the particle concentration indicated by the CNC was much greater than $10^6/cm^3$. Coagulation quickly ensued, and particle diameter in this experiment was therefore larger than that observed in the first experiment.

Comparison between the two methods remains impossible 30 min after the production of particles. As stated previously, the size distribution at this point is concentrated in the first two channels of the EAA.

Figure 11 compares the real size distribution ~4 h after the production of particles, with allowance for counting loss. At this time, the large particles resulting from coagulation have appeared, and only a few, stable small particles remain, having no opportunity to coagulate. As has already been seen, comparison is not satisfactory in this small-particle range. For $d \geq 0.04$ μm, agreement between the two methods seems to be good.

Experiment 3: bimodal size distribution — After radioactive gas is first injected, a unimodal particle size distribution is observed (Figure 12). It has a maximum value which moves with time to increasing radii, the amplitude of this maximum decreasing as a function of time. The number of larger particles increases as the number of the smaller ones decreases, as a result of coagulation.

About 5 min after a second injection of actinon, the particle size distribution becomes bimodal, as represented by Figure 13. The first mode reflects the small particles created by radiolysis. The second mode represents the particles already present at the time of the second injection of actinon. In time, the particle size distribution again becomes unimodal.

Comparison of the methods is again found unsatisfactory in the range of small particles, but good in the range of larger particles ($d > 0.02$ μm).

Photolysis Aerosol

Experimental Device —

It seemed interesting to extend this work to the case of an aerosol continuously produced by photolysis of sulfur dioxide (SO_2). It is now established that photooxidation of atmospheric SO_2 leads to the production of sulfuric acid and sulfates, usually found in the form of submicronic particles; it is thus extremely important to understand the evolution of these particles in order to characterize atmospheric pollution.

Our experimental device for producing particles, similar to the preceding one, contains a spherical chamber of 800-liter volume maintained in darkness, a system for injecting SO_2 into the chamber, and a high pressure mercury vapor lamp.

Sulfur dioxide was transformed into sulfate, providing for the system a continuous production of particles. This continuous production, which governs further evolution of the aerosol system, can be modified by varying the SO_2 concentration injected into the spherical chamber.

In addition, the diffusion battery of rectangular plates was replaced with a Sinclair 11-stage cylindrical battery. Each stage is a plate having a bundle of circular holes of equal diameter; here, Equation (6) can be applied. The tubes in this battery are of honeycomb structure with a total of 9,750 holes in each plate; the total equivalent length of the device is 3,374 meters. Each of the 11 sample ports connects to a solenoid valve, opening to a common collector, resulting in the same symmetrical structure for each unit. Individual battery tube lengths are listed below.

Tube	Length (cm)
1	0.3175
2	0.3175
3	0.635
4	0.9525
5	1.270
6	1.905
7	2.540
8	3.810
9	5.080
10	7.620
11	10.160

The flow rate through the battery is 4 liters/min.

Using Equation (6) the attenuation at each stage was calculated for a given particle radius. Theoretical results were compared to experimental values with the 11-stage battery traversed by a monodisperse aerosol, obtained with the electrical classifier of Liu and Pui (11). The comparison is given in Figure 14.

The size distribution of a given polydisperse aerosol is determined by the Maigne method, modified for a battery of cylindrical canals. The variable is not the total flow rate, maintained constant at 4 liters/min, but the lengths of successive tubes. Counting losses of the instrument (Formula 15) are taken into account.

Results —

Figure 15 represents the evolution of the real-number size distribution obtained by the DBM (allowing for counting losses of the CNC). The initial moment in time is defined as the instant when SO_2 is introduced into the reaction chamber and irradiation takes place. The DBM is seen to allow access to the ultrafine part of the size range (<0.01 μm). Thirty minutes after the experiment begins, the size distribution is unimodal. A fraction of particles is assumed below the detection limit of the CNC, estimated to be d = 0.0018 μm. After 1 h, particles with d > 0.01 μm appear, issuing from coagulation of the smaller particles. Measurements carried out after 3 h show the ultrafine fraction of the size distribution remains, but a second mode develops with a tendency for large diameters. It is notable that the size distribution is qualitatively comparable to the one foreseen by Walter (17).

Figure 16 shows: 1) the number concentration, 2) the total surface area, and 3) the total volume as a function of time, measured by the DBM. For ~1 h, particle evolution is governed essentially by nuclei formation through homogeneous nucleation: a rapid growth of the three parameters characterizing the aerosol is seen. The concentration reaches n_{max} when equilibrium is achieved between nucleation and coagulation, then slowly decreases as numbers are lost in coagulation. The curves of Figure 16 indicate the volume remains appreciably constant after 1 h of irradiation, whereas the surface tends to decrease slightly in the same time period. For comparison, Boulaud (18) recently described an evolution model for sulfuric acid vapor in an atmospheric aerosol. Our experiments, with a production rate of vapor molecules at $10^6/cm^3/sec$ and a surface area of 600 $\mu m^2/cm^3$, would take place in a range of uncertainty in the Boulaud model, where homogeneous nucleation and vapor condensation on the particles are likely to intervene. This is confirmed by the behavior of the size distribution represented by Figure 15.

Comparison Between the Results of EAA and DBM —

Figures 17 and 18 compare the number size distributions obtained by EAA and DBM, 1 and 3 h after irradiation is begun. With these experiments, the SO_2 concentration was increased, leading to a higher molecule production rate ($10^8/cm^3/sec$). As we have already seen, the electrical analyzer is not useful

for the small aerosol range (d < 0.01 μm), since the small particle size is not within the detection limit of this instrument. For particles with d > 0.01 μm, both methods give comparable results, while the size distribution shape remains the same.

Figure 19 represents as a function of time: Curve A) the concentration indicated by the CNC, Curve B) the real concentration taking into account the counting losses in this instrument, and Curve C) the concentration given by the EAA. Using these curves, it is possible to appreciate the importance of counting losses in the CNC, which are fairly large at the beginning of irradiation and remain evident later on. This confirms the hypothesis that homogeneous nucleation does not stop. After 1 h, the evolution of the curves is similar; a slow decrease, caused by losses due to coagulation, is noticeable.

Figure 20 represents: Curve A) the total volume calculated by the DBM, Curve B) the volume of particles with d > 0.01 μm, and Curve C) the total volume measured by the EAA. Similarly, the corresponding surfaces are shown (Figure 21). Curves B and C in Figures 20 and 21 show that both methods used provide comparable results, while the difference can result from measurement uncertainties inherent in each technique. It can be seen that the volume increases regularly and the surface reaches an almost constant value after 1 h of irradiation. In this particular case, McMurry (19) and McMurry and Friedlander (20), using the theory of self-preserving distribution, assert that the development of a "self preserving surface" proportional to 3/5 power of the variation in volume is foreseeable. For their calculations, it would be possible to obtain after 100 min a total surface of 400 $\mu m^2/cm^3$. This volume is very close to that measured experimentally (Figure 21, Curve B), when no account is taken of particles in the range of d < 0.01 μm, that is, when the real surface of the aerosol is minimized.

Curves A and B in Figures 20 and 21, therefore, indicate the importance of ultrasmall particles. This part of the range (d < 0.01 μm) is seen to contribute very little to the total aerosol volume, but it plays an appreciable

role in the total surface area. Since nuclei with d < 0.01 μm have previously been ignored, some distortion may have arisen in calculations involving heterogeneous nucleation based on evaluation of the available aerosol surface.

Furthermore, with vapor molecule production rate of $10^8/cm^3/sec$ and a total surface of 10^3 $\mu m^2/cm^3$, according to Boulaud (18), conditions are favorable for nucleation. This is confirmed by our experimental results. On the one hand, the Figure 18 curves obtained by DBM show that small particles, originating with homogeneous nucleation, remain. Similarly, comparison of Curves A and B of Figures 20 and 21 shows the importance of very small particles. On the other hand, although the phenomenon of coagulation theoretically reduces the total surface and preserves the total volume of aerosol, we have seen in Figure 20 and 21 that the surface area remains practically constant, whereas the volume increases regularly. This results essentially from vapor contribution by condensation on existing particles.

These theoretical and experimental considerations thus lead to the conclusion that a competition exists between phenomena of homogeneous and heterogeneous nucleation in development of the aerosol studied.

COMPARISON WITH NATURAL AEROSOL

Experimental Device

The experimental device was modified to study atmospheric aerosol by both methods, EAA and DBM. Measurements to determine size distributions require a time of about 4 to 5 min by either method. Because of ambient aerosol fluctuations, direct measurements in the atmosphere were not possible. A sampling device suitable for measurements was perfected, consisting mainly of a tight, metallic volume surrounding a plastic envelope that can inflate or deflate. This constitutes an aerosol sampling bag. The aerosol sampling is achieved in three stages:

1) Emptying the bag by collapsing it

2) Sampling aerosol into the bag by applying suction between the bag and metallic shell

3) Analysis.

During the analysis stage, aspiration by the analyzers (EAA or DBM coupled with a CNC) causes a contraction of the plastic envelope; but no change in the concentration occurs, which is absolutely necessary for either method to satisfactorily determine the size distribution.

This device permits preparation of dilutions in a known ratio and is suitable for in situ measurements for different typical aerosols encountered in different conditions. The size distribution of the ambient aerosol outside our laboratory at Fontenay-aux-Roses was studied in May 1979.

Figure 22 represents the attenuation measured at each of the 11 stages of the cylindrical diffusion battery used in the photolytic study and described above. Each curve is obtained at a different time in the day.

Results

Figure 23 represents the evolution of the number distribution at 4:30, 7:30, and 9:00 a.m. At 4:30, just before sunrise, the distribution has a mean geometric diameter of 0.065 μm and a standard deviation equal to 1.5. At 7:30, after sunrise, the number of particles with $d < 0.1$ μm clearly increases because of the presence of new particles generated by gas-to-particle conversion. At 9:00, particles with $d < 0.01$ μm disappear, causing an increase in particles with $d = 0.01$ to 0.1 μm. One can attribute this increase to the coagulation and condensation of H_2SO_4 processes.

These curves are not comparable to the first curve of Figure 15, corresponding to artificial photolysis, because the concentration of particles is about 10 times less than in the artificial case (Irradiation intensity and SO_2 concentration differ in the two cases).

Comparison Between DBM and EAA

Figures 24 and 25 give the comparison between the results obtained simultaneously with DBM and EAA. As already stated, indications given by the two techniques are in good agreement for particles in the range of $d > 0.01$ µm. For 0.002 µm $< d < 0.01$ µm, only the DBM seems to produce usable data.

Figure 26 represents as a function of time the real concentration given by the DBM, taking into account the counting loss of the CNC. This curve corresponds to Curve B in Figure 19, where concentration measurements by three different methods were established as a function of time. These curves are not comparable to the curve of Figure 26. Complete discussion should be based on more numerical results, for which calculations are under way. In addition, natural conditions (in particular, concentration of particles) seem to differ significantly from the conditions for measurement by artificial photolysis, described above.

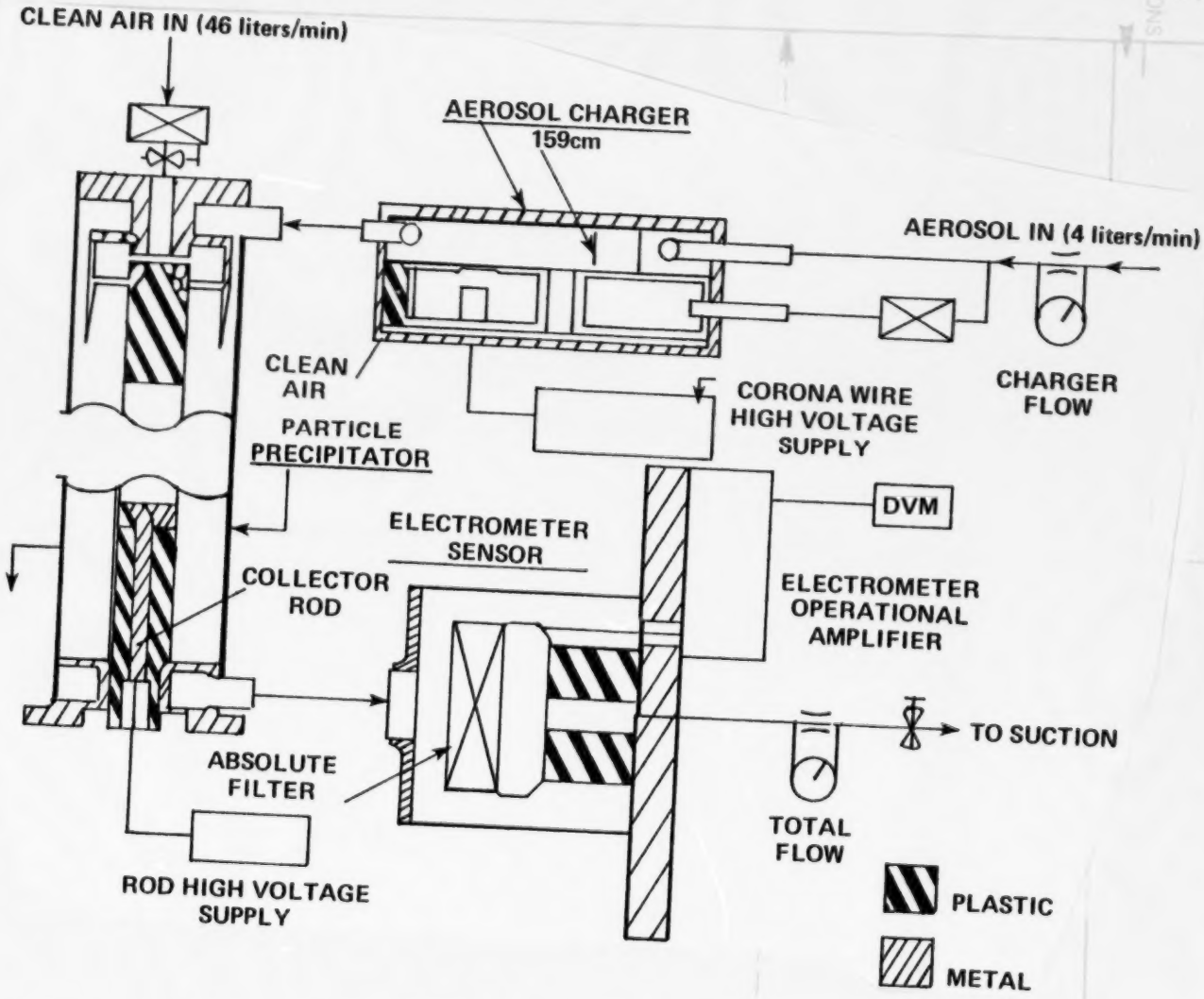

Figure 1. Schematic system diagram of the EAA.

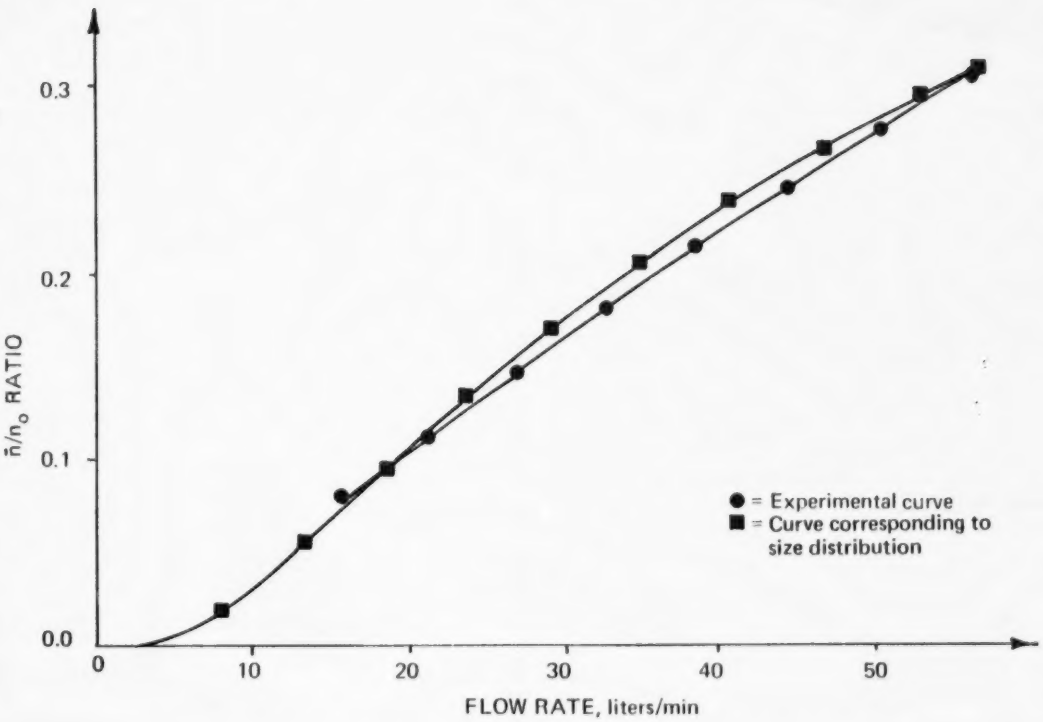

Figure 2. Variation in $\bar{n}/n_o$ ratio as a function of flow rate.

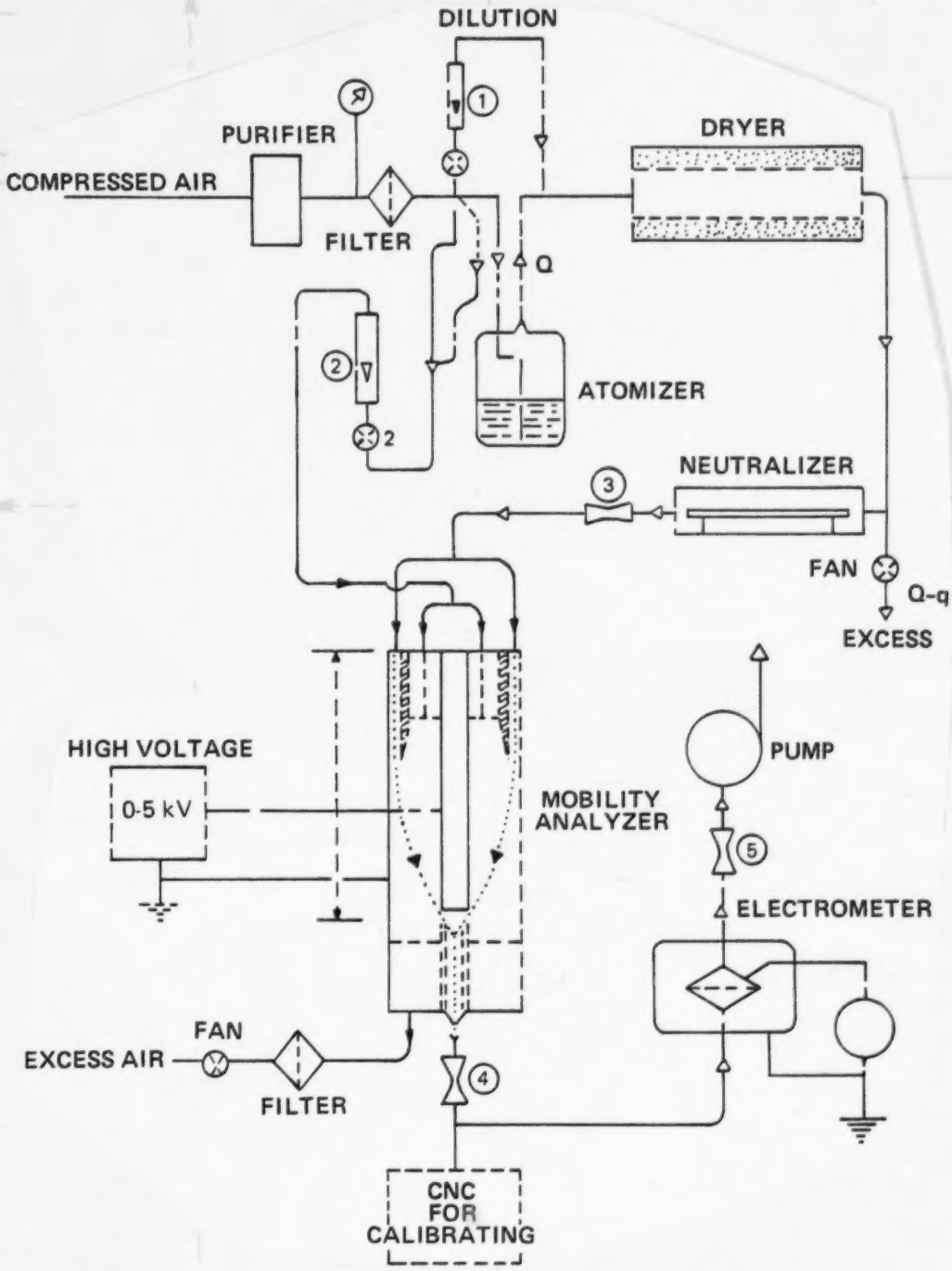

Figure 3. Aerosol generator.

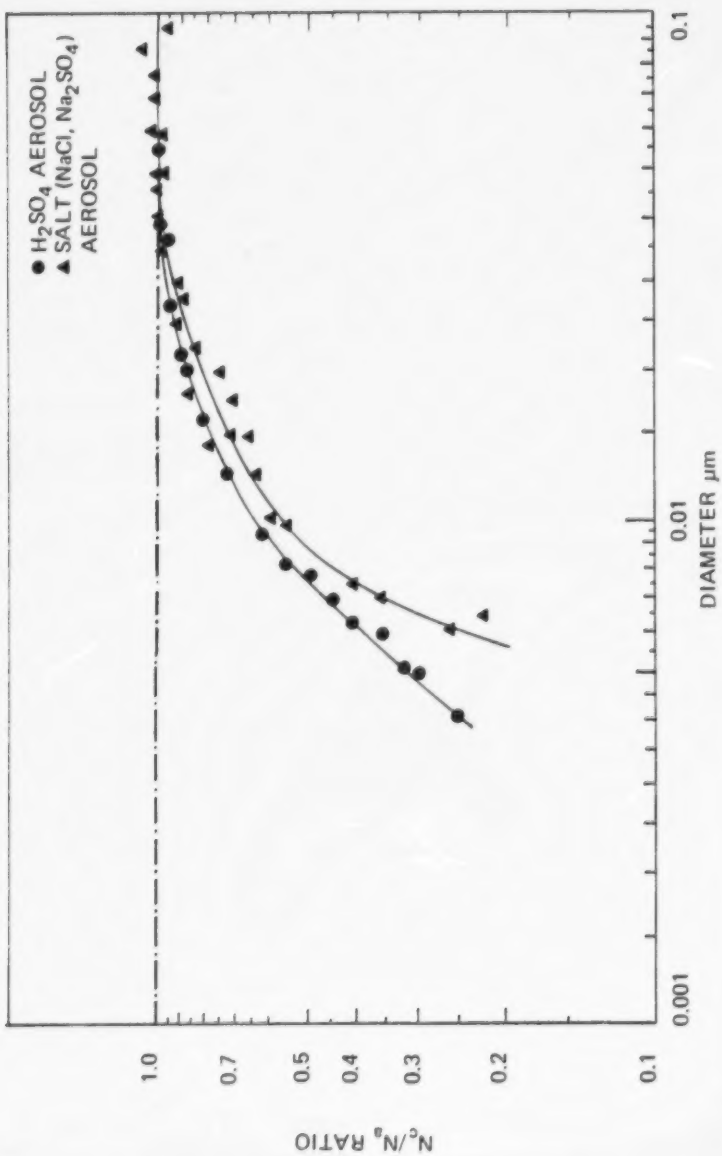

Figure 4. Variation in N_c/N_a ratio for varying diameter size.

BEGIN FIRST LINE OF TEXT HERE
TYPING GUIDE SHEET
CENTER OF PAGE
TOP OF IMAGE AREA
DROPPED HEAD; BEGIN SECTIONS HERE

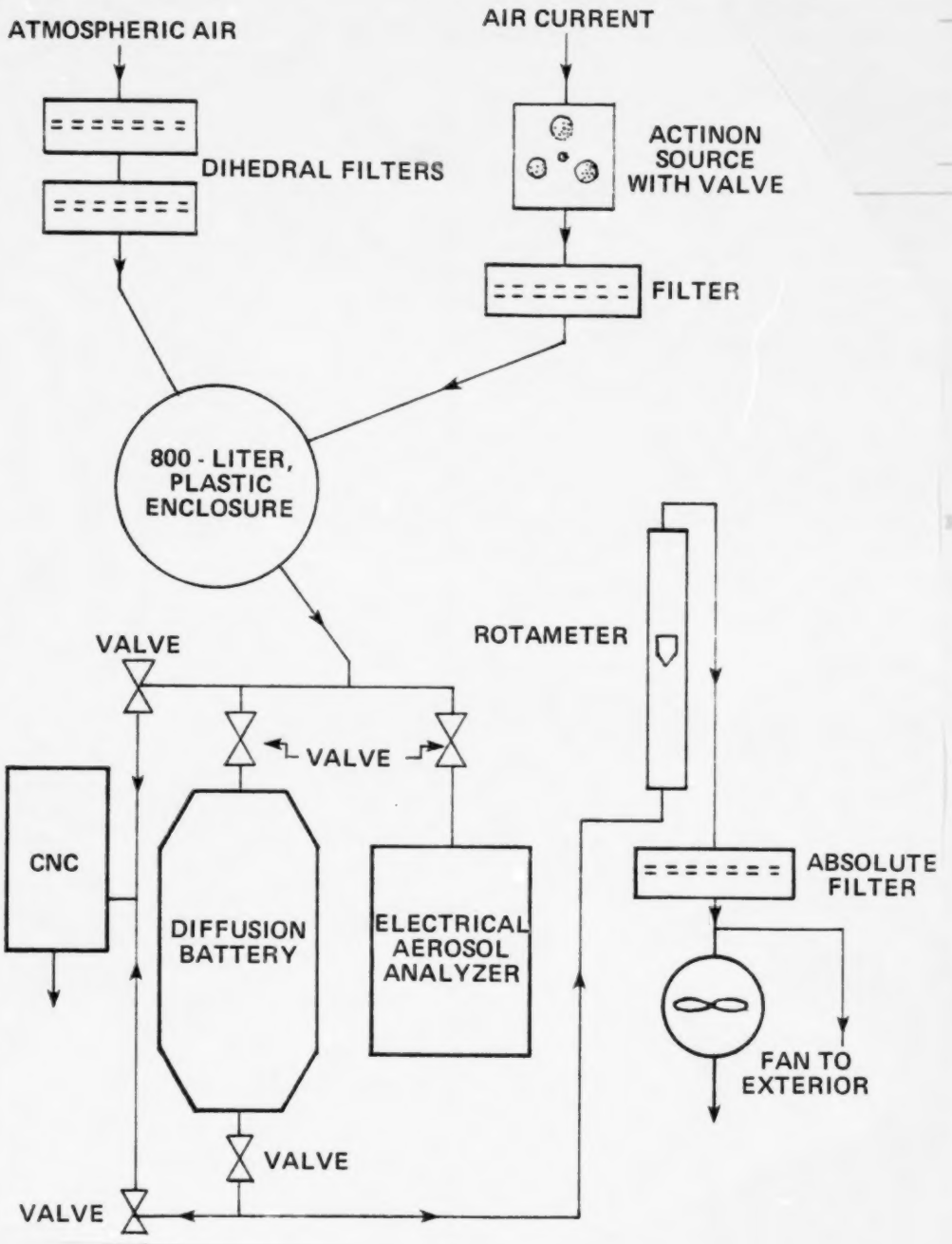

Figure 5. Experimental device for radiolysis experiment.

BEGIN LAST LINE OF TEXT
BOTTOM OF IMAGE AREA, OUTSIDE DIMENSION FOR TABLES AND ILLUSTRATIONS
3/8"

PAGE NUMBER
EPA-287 (Cin.)
(4-76)

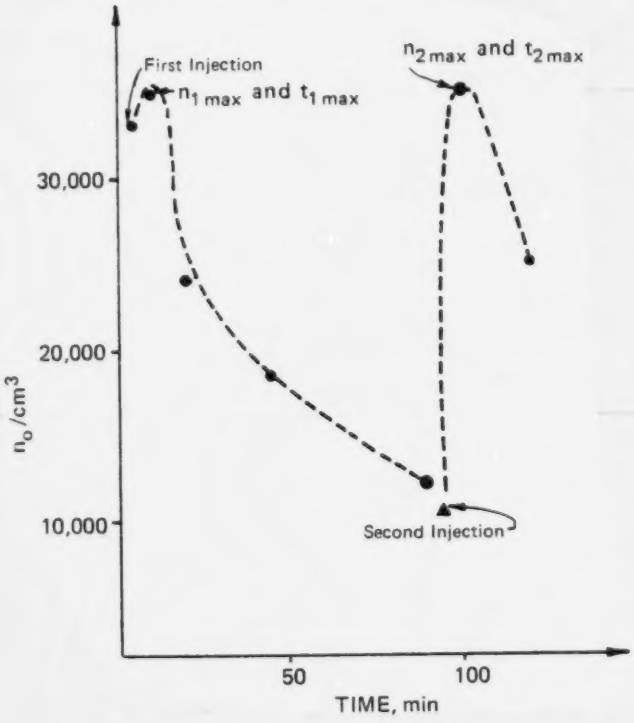

Figure 6. Variation in "apparent" particle number as a function of time, according to DBM measurements.

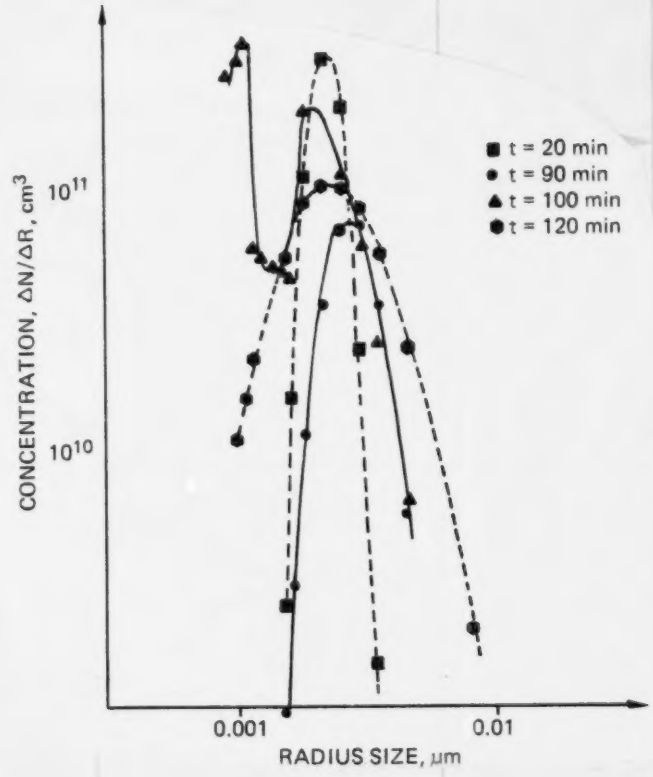

Figure 7. Variation in time of particle size, according to CNC measurements, and corrected for counting losses.

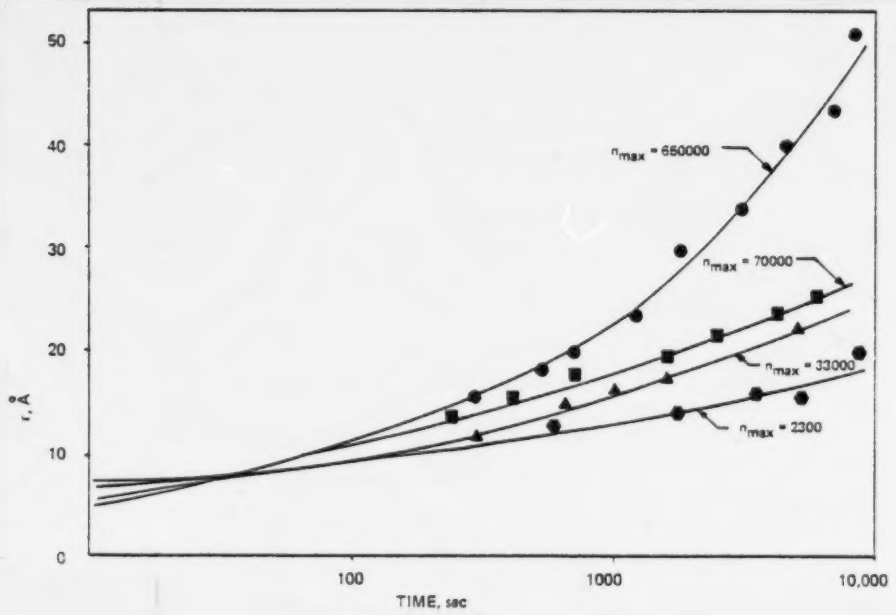

Figure 8. Variation as a function of time in "apparent" radius produced by radiolysis, for different values of n_{max}.

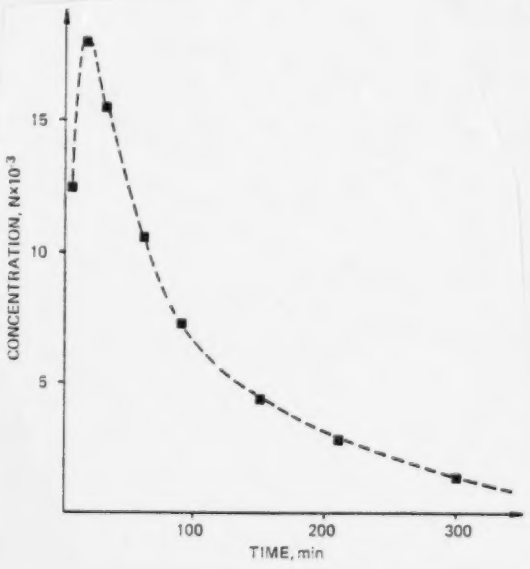

Figure 9. Evolution with time of "apparent" total particle concentration, as indicated by CNC.

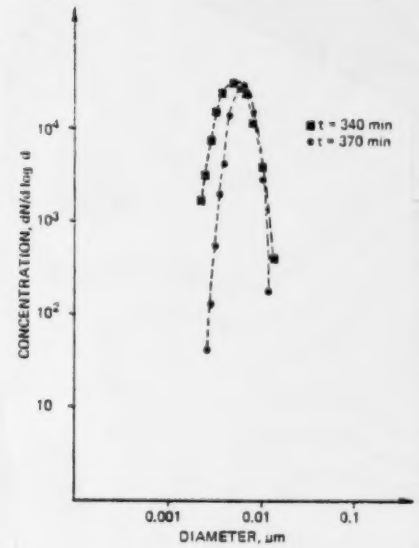

Figure 10. Size distribution obtained by DBM at two different times.

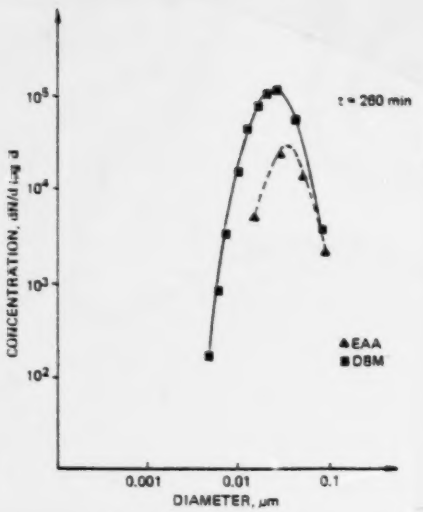

Figure 11. Size distributions obtained by DBM and EAA after 4 h.

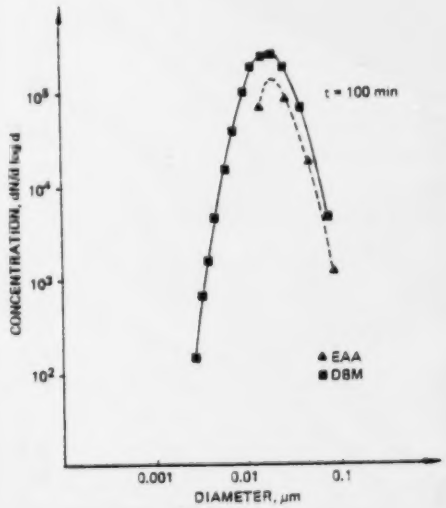

Figure 12. Size distributions obtained by DBM and EAA after 2 h.

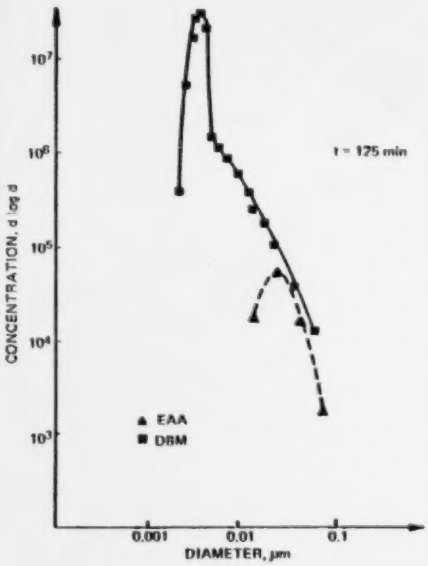

Figure 13. Bimodal size distributions obtained by DBM and EAA.

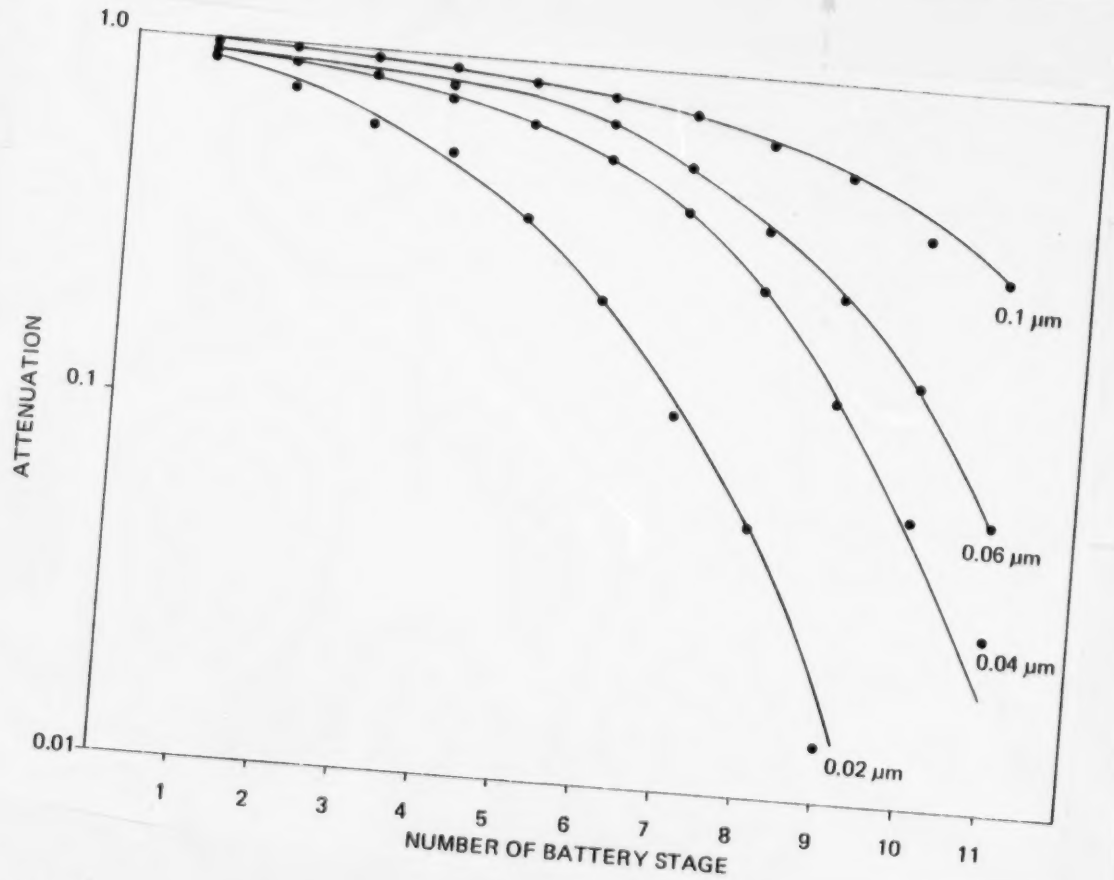

Figure 14. Calculated v. measured attenuation at each battery stage for four diameter sizes.

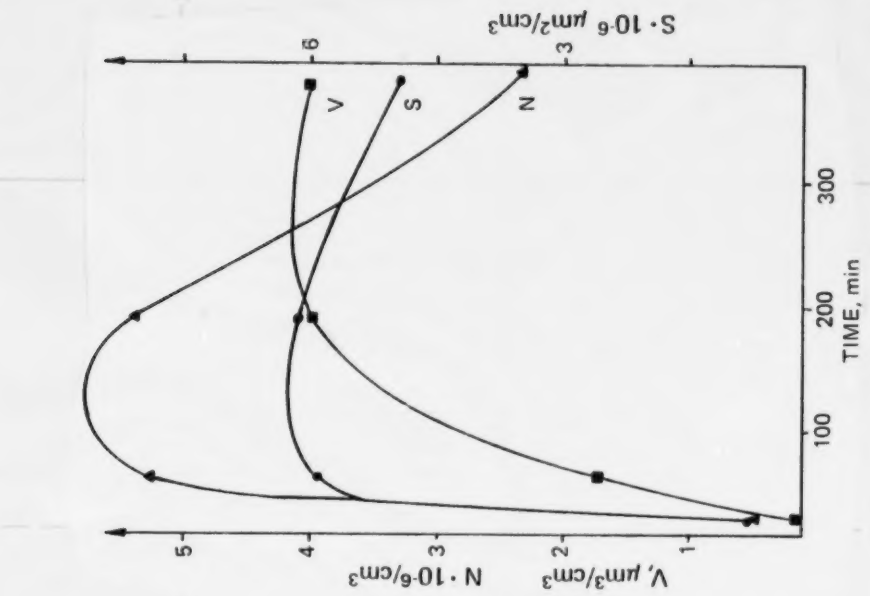

Figure 16. Variation as a function of time in number, surface, and volume, measured by DBM.

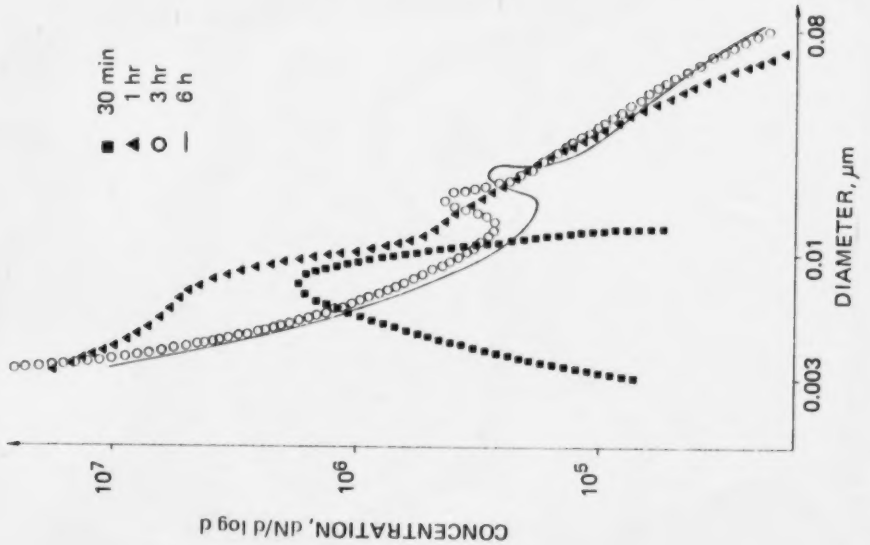

Figure 15. Evolution of real number/size distribution obtained by DBM.

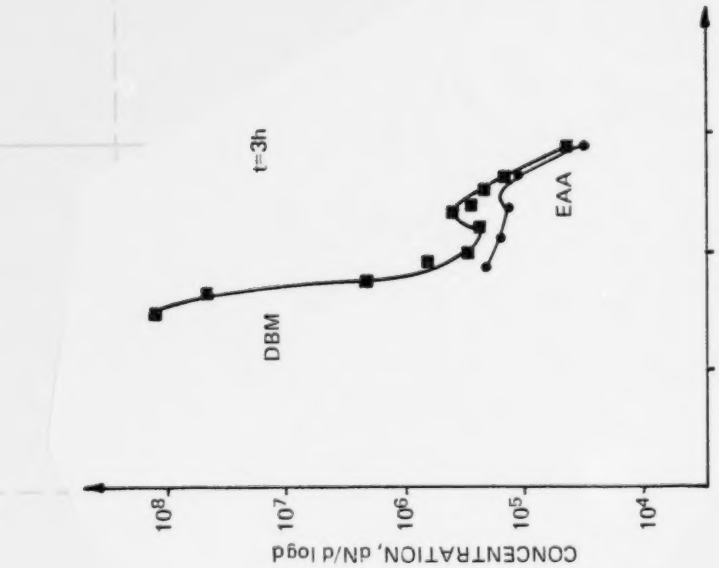

Figure 18. Number/size distribution 3 h after irradiation, measured by EAA and DBM.

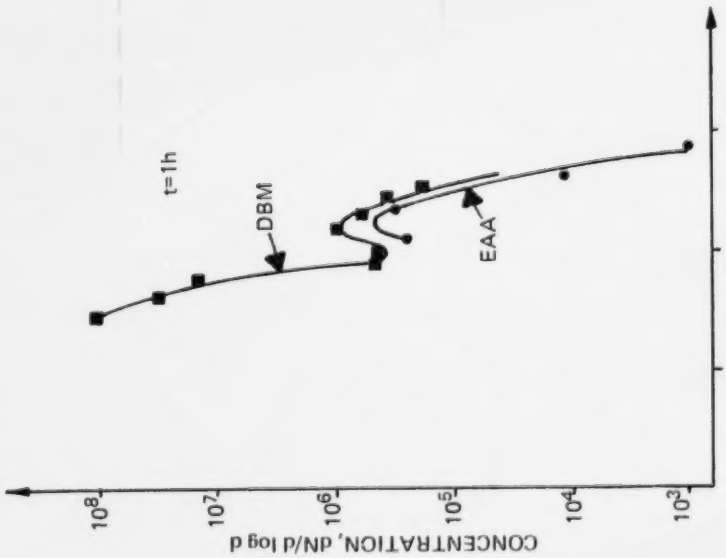

Figure 17. Number/size distribution 1 h after irradiation, measured by EAA and DBM.

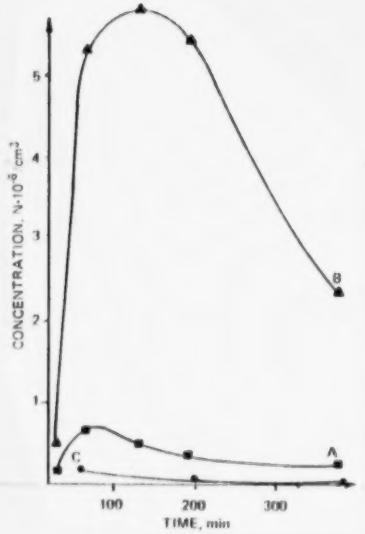

Figure 19. Concentration as a function of time: Curve A) as indicated by CNC, Curve B) corrected for CNC counting losses, Curve C) as indicated by EAA.

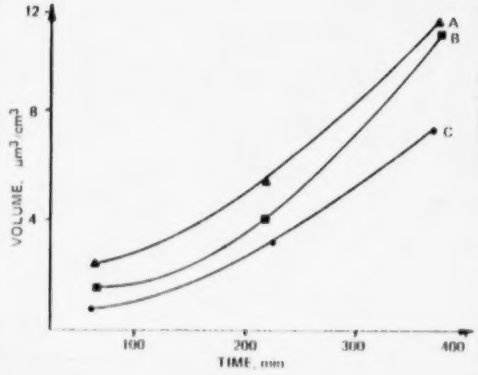

Figure 20. Volume as a function of time: Curve A) as indicated by DBM, Curve B) of particles with d < 0.01 µm, Curve C) as indicated by EAA.

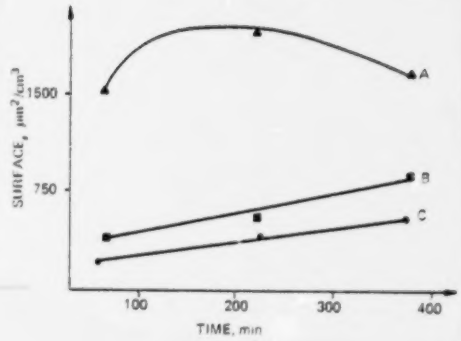

Figure 21. Surface area as a function of time: Curve A) as indicated by DBM, Curve B) of particles with d > 0.01 µm, Curve C) as indicated by EAA.

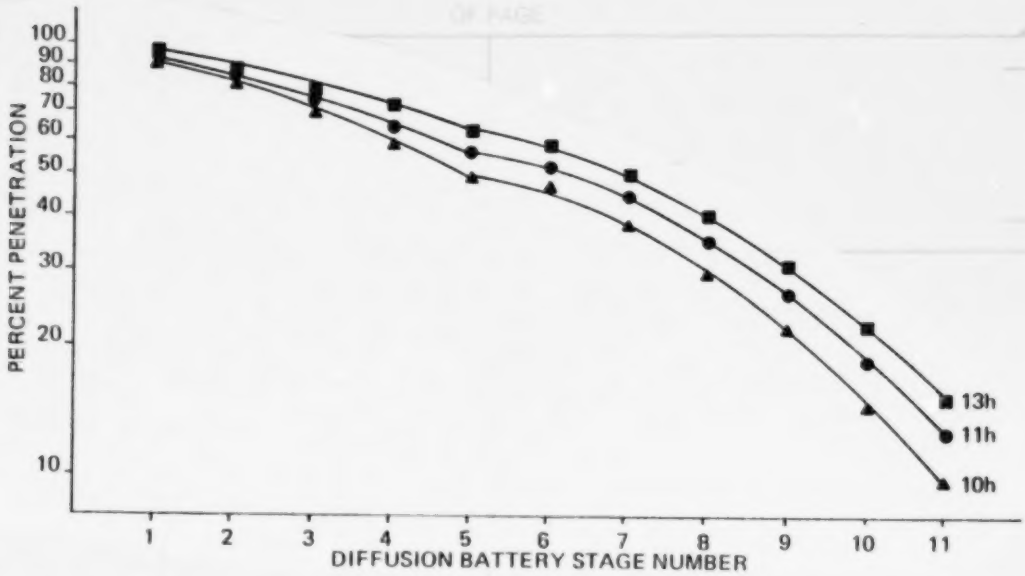

Figure 22. Percent of particles penetrating to each of the 11 stages at 3 different times of day.

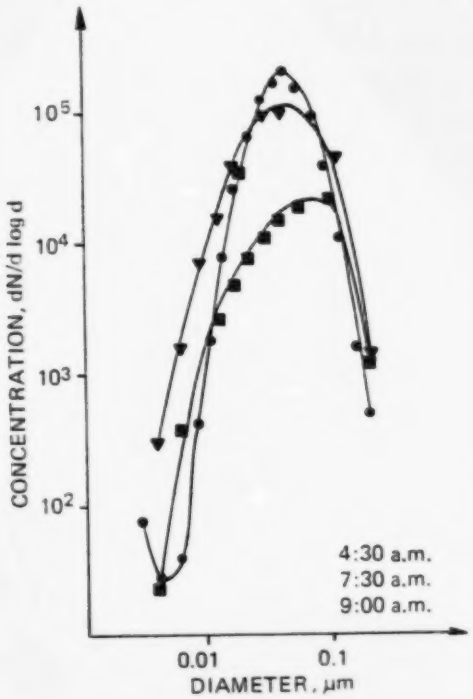

Figure 23. Variation with time in the number/size distribution of natural aerosol.

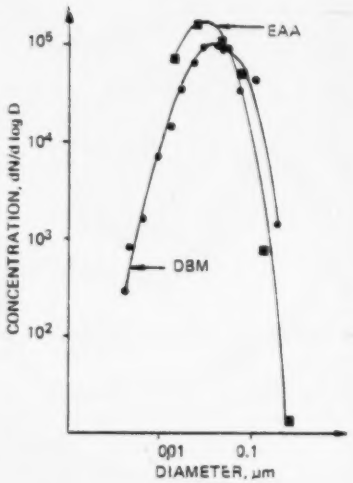

Figure 24. Comparison of number/size distribution measurements with EAA and DBM at 7:30 am.

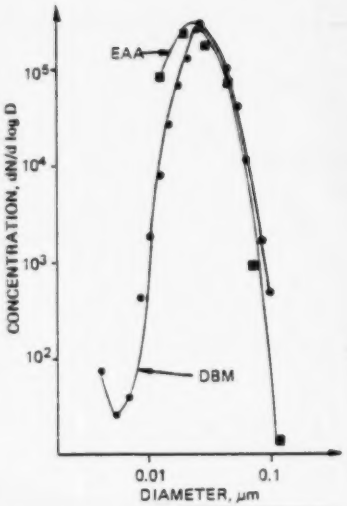

Figure 25. Comparison of number/size distribution measurements with EAA and DBM at 9:00 am.

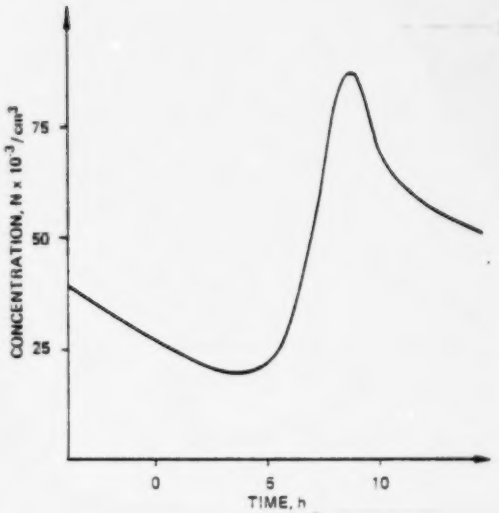

Figure 26. Concentration as a function of time, corrected for counting losses, as indicated by DBM.

REFERENCES

1. Liu, B. Y. H., K. T. Whitby, and D. Y. H. Pui. JAPCA, 24(14):1067, 1974.

2. Whitby, K. T., and B. Y. H. Liu. Atm. Env., 2:103, 1968.

3. Whitby, K. T., and W. E. Clark. Tellus, 18:573, 1966.

4. Bademosi, F. PhD. Thesis, Minneapolis, Minnesota, 1971.

5. Gormley, P. G., and M. Kennedy. Proc. Royal Irish Acad., 52:163, 1949.

6. Marcus, W. de, and J. W. Thomas. J. U.S. AEC, ORNL, 1413, 1952.

7. Thomas, J. W. J. Colloid and Interface Sci., 10:246, 1955

8. Twomey, S. J. Franklin Inst., 215:121, 1963.

9. Maigne, J. P. PhD. Thesis, Paris, 1976.

10. Maigne, J. P., P. Y. Turpin, G. Madelaine, and J. Bricard. J. Aerosol Sci., 5:339, 1974.

11. Liu, B. Y. H., and D. Y. H. Pui. J. Colloid and Interface Sci., 47(1): 155-171, 1974.

12. Bricard, J., G. Madelaine, and M. L. Perrin. International Conference on Condensation Nuclei, Galway, 1977.

13. Liu, B. Y. H., and C. S. Kim. Atm. Env., 11:1097, 1977.

14. Liu, B. Y. H., and D. Y. H. Pui. J. Aerosol Sci., 5:465, 1974.

15. Mirabel, P., and J. L. Katz. J. Chem. Phys., 60:1138, 1974.

16. Takahashi, T., M. Kasahara, and M. Itoh. J. Aerosol Sci., 6:45, 1975.

17. Walter, H. J. Aerosol Sci., 4:1, 1973.

18. Boulaud, D. PhD. Thesis, Paris, 1976.

19. McMurry, P. H. PhD Dissertation, California Inst. Technol., 1977.

20. McMurry, P. H., and S. K. Friedlander. J. Colloid and Interface Sci., 64(2):248-257, 1978.

APPENDIX A

ALGORITHM TO SOLVE SYSTEM OF N EQUATIONS

FORMATION AND USE OF M SYSTEM

The spectrum of the aerosol under study was divided into N classes, D_1D_2, D_2D_3 ... D_ND_{N+1}. We superimpose on the N classes a more approximate categorizing into M classes, $D'_1D'_2$ ... $D'_MD'_{M+1}$ ($M < N$) so that

$$D'_1 = D_1 \text{ ..... } D'_{M+1}\ D_{N+1}$$

Each D_jD_{j+1} class comprises K_j successive classes from the first, N classification, where $1 < K_j < N$. We can write (Figure 1A)

$$\text{segment } D'_j\ D'_{j+1} = \text{segment } D_k\ D_{k+K_j} = \sum_{i=K}^{k+k_j-1} D_iD_{i+1} \text{ classes}$$

We introduce this simplification only for the case of the flat battery. In this case, 11 measurements are available; 4 measurements, each separated by 3 points, are used. The total flow rate varies between 6 and 56 liters/min. For the cylindrical battery, the 11 measurements and the upstream concentration measurement are used, and a constant total flow rate of 4 liters/min is maintained.

The following limitation is introduced: On each segment $D'_jD'_{j+1}$, the size distribution of the corresponding aerosol is assumed lognormal. In other words, on each segment $D'_jD'_{j+1}$ the parameters d_{gj} and s_{gj} are defined, representing respectively the mean geometric diameter and standard deviation of

the lognormal size distribution; these provide an approximation, on the segment $D_j D_{j+1}$, of the real distribution of the aerosol under study. Regardless of the real size distribution of an aerosol, it is reasonable to transform different portions of this distribution to lognormal distribution elements, if the number of elements is sufficiently large.

To the segments $D_1 D_2 \ldots D_N D_{N+1}$ and $D'_1 D'_2 \ldots D'_M D'_{M+1}$ we associate the parameter values α (depending on the flow rate or the length): $\alpha_1, \alpha_2 \ldots \alpha_N$ and $\alpha'_1 \alpha'_2 \ldots \alpha'_M$, respectively, to which the measurements $\bar{n}/n_o \ldots \bar{n}_N/n_o$ and $\bar{n}'_N/n_o \ldots \bar{n}_M/n_o$ correspond. To each diffusion coefficient is associated a corresponding diameter, d_{N+2-i} and d'_{M+2-j} (Figure 1A).

Let

$$Y'_i = Y_i \frac{D_{i+1} - D_i}{n_o} \qquad L = 1 \ldots N$$

the fraction $D_i \ldots D_{i+1}$ taken from the total spectrum. We can write:

$$\frac{\bar{n}_i}{n_o} = \sum_{j=1}^{i} X'_{ij} Y'_j$$

with

$$X'_{ij} = \frac{X_{ij}}{D_{j+1} - D_j}$$

The method consists of superimposing Y'_1 on interval $D_i D_{i+1}$, constituting segment $D'_j D'_{j+1}$ in a lognormal distribution. It results that

$$Y'_i = P\left(Z_{(N+2) - (i+1)}\right) = Y'_i (d_{gj}, \sigma_{gj}) \qquad \text{(A-1)}$$

with

$$P(Z_h) = \frac{1}{2\pi} \int_{-\infty}^{Z_h} e^{-z^2} dz \qquad \text{(A-2)}$$

and

$$z = \frac{\log_{10} d - \log_{10} d_{gj}}{\log_{10} \sigma_{gj}} \qquad \text{(A-3)}$$

i being variable between (Figure 1A) $K_1 + K_2 + \ldots K_{j-1}$ and $K_1 + K_2 + \ldots K_j$. The unknown N quantities are not now independent, and for $i = 1 \ldots K_1$

$$\frac{\bar{n}_i}{n_o} = \sum_{k=1}^{i} X'_{ik}\, Y'_k\, (g_{g_1}, \sigma_{g_1})$$

$$\vdots$$

For $i = K_1 + K_2 + \ldots K_{j-1}, K_1 + K_2 + \ldots K_j$

$$\frac{\bar{n}_i}{n_o} = \sum_{k=1}^{K_1} X'_{ik}\, Y'_k\, (d_{g_1}\, \sigma_{g_1}) + \ldots \sum_{k=K_1+K_2+\ldots K_{j-1}}^{i} X'_{ik} Y'_k\, (d_{gj}, \sigma_{gj})$$

$$\vdots$$

For $i = K_1 + K_2 + \ldots K_{M-1} + 1, K_1 + K_2 + \ldots K_M$

$$\frac{\bar{n}_i}{n_o} = \sum_{k=1}^{K_1} (X'_{ik}\, Y'_k)\, (d_1, \sigma_{g_1}) + \ldots \sum_{k=K_1+K_2+\ldots K_{M-1}+1}^{i} X'_{ik} Y'_k\, (d_{gM}, \sigma_{gM}) \qquad \text{(A-4)}$$

To the above system, the M-1 relations are added, resulting in continuity conditions for segments adjoining $D'_j D'_{j+1}$

$$\frac{\log_{10} d'_{M+2-j} - \log_{10} d_{gj}}{\sigma_{gj}} = \frac{\log_{10} d'_{M+2-j} - \log_{10} d_{g\,j-1}}{\sigma_{g\,j-1}} \qquad \text{(A-5)}$$

for $j = 2 \ldots M$.

The above relations show that the two M variables, d_{gj} and σ_{gj}, are not independent, and they can be written as functions of the M+1 independent variables $d_{g1} \ldots d_{gj}\ \sigma_{g1}$. Theoretically, σ_{g1} could be suppressed if D_1 and the upper limit, $d_{N+1} = d'_{M+1}$, could be determined with sufficient certainty, but our method lacks this precision. For this reason, we assume that d_{N+1} and D_1 are known. That is the only hypothesis to be made concerning the aerosol in question. In these conditions d_{g1} and σ_{g1} are dependent. We can determine the value $P\ (z_{N+1})$ where

$$z_{N+1} = \frac{\log_{10} d_{N+1} - \log_{10} d_1}{\log_{10}\ \sigma_{g_1}} \qquad \text{(A-6)}$$

up to the value $P\ (z_{N+1}) = 0.999$, and where all particles have $d < d_{N+1}$; $P(Z_{N+1})$ cannot be used, because $P(z)$ reaches this limit for $d = \infty$. Using the value 0.999 implies that particles with $d > d_{N+1}$ do not exist. Corresponding to this value for d_{N+1} is $z_{N+1} = 3.72$. It results that

$$3.72 = \frac{\log_{10} d_{N+1} - \log d_{g1}}{\log_{10} \sigma_{g1}} \qquad \text{(A-7)}$$

The N variables Y'_i, which are not independent, depend only on the M independent variables.

CALCULATED VS. MEASURED VALUES

In the Gaussian log diagram of Figure 2A, let M+1 be the point 99.99 percent, d'_{M+1} already having been defined. Rather than the N measurements $\bar{n}_o/n_o$ $(i = 1 \ldots N)$, we are primarily interested in M measurements $(\bar{n}'_j/n_o,\ j = 1 \ldots M)$ corresponding to the classification $D'_1, D'_2 \ldots D'_{M+1}$. We determine d_{g1} (σ_{g1} depends on d_{g1}), based on knowledge of the point M+1, so that the quantity

$$\frac{\sum_{i=1}^{K_1} X'_{K_1 i}\, Y'_i\, (d_{g_1}) - \frac{\bar{n}_{K_1}}{n_o}}{\frac{\bar{n}_{K_1}}{n_o}} \qquad \text{(A-8)}$$

is less than 0.001. That is the relative deviation between the calculated and measured value. In Figure 2A, point M+1 is fixed, and the corresponding d_{g1} is determined in agreement with the above condition.

In the diagram of Figure 3A is seen experimental curve I ($\bar{n}/n_o$) versus Q, and the calculated curve I_1 ($\bar{n}/n_o$) versus Q, defined by log d_{g1} according to Equation (A-7).

To obtain a better approximation of experimental curve I, accounting for the possible error in the measured $\bar{n}_K/n_o$, we estimate the error to be 5 percent. A segment $A_{K_1}\ B_{K_1}$, parallel to the ordinate axis, is defined; and point C_{K_1} of this segment, adjustable to 0.001, (if it exists) must be determined. In other words, point C_{K_1} is determined such that (Figure 3A)

$$\frac{\sum_{i=1}^{K_1} X'_{K_1,i}\, Y'_i\, d_{g_1}(C_{K_1}) - \frac{\bar{n}_{K_1}\ (CC_{K_1})}{n_o}}{\frac{\bar{n}_{K_1}}{n_o}\ (C_{K_1})} < 0.001 \qquad \text{(A-9)}$$

and

$$\frac{\sum_{i=1}^{N} N'_{K_1} + \ldots K_{N,i}\, d_{g_1}(C_{K_1}) - \frac{\bar{n}_N}{n_o}}{\frac{\bar{n}_K}{n_o}} \qquad \text{(A-10)}$$

is minimum.

In the diagram of Figure 3A, Curve I_2 is obtained, corresponding to the lognormal distribution $d_{g_1}(C_{K_1})$, closer of I than to I_1. In this case, the solution defined by $\log d_{g_1}$ and C_{K_1} is always available.

To depart from calculation, we utilize, from among the Y'_i $(i = 1, N)$ of the lognormal distribution characterized by $d_{g_1}(C_{K_1})$, the Y'_i $(i = 1, K_1)$. By the above process, we investigate d_{g_2} such that (Figure 4A)

$$\frac{\sum_{i=1}^{K_1} X'_{K_1+K_2,i} Y'_i d_{g_1}(C_{K_1}) + \sum_{i=K_1+1}^{K_1+K_2} X'_{K_1+K_2,i} Y'_i (D_{g_2}) - \frac{\bar{n}_{K_1+K_2}}{n_o}}{\bar{n}_{K_1+K_2} \Big/ n_o} \tag{A-11}$$

would be less than 0.001, and $d_{g_2}(C_{K_2})$ must be determined such that

$$\frac{\sum_{i=1}^{K_1} X'_{K_1+K_2,i} Y'_i d_{g_1}(C_{K_1}) + \sum_{i=K_1+1}^{K_1+K_2} X'_{K_1+K_2,i} Y'_i d_{g_2}(C_{K_2}) - \frac{\bar{n}_{K_1+K_2}(C_{K_2})}{n_o}}{\bar{n}_{K_1+K_2} \Big/ n_o} \tag{A-12}$$

would be less than 0.001, and

$$\frac{\sum_{i=1}^{K_1} X'_{K_1+\ldots K_M,i} Y'_i d_{g_1}(C_{K_1}) + \sum_{i=K_1+1}^{N} X'_{K_1+\ldots K_M,i} Y'_i d_{g_2}(C_{K_2}) - \frac{\bar{n}_N}{n_o}}{\bar{n}_N \Big/ n_o} \tag{A-13}$$

is minimum.

The first equations above give d_{g_2} and I_3, which may exist or not. If $d_{g_2}(C_{K_2})$ exists, we have or do not have Curve I_4 (Figure 4A). If I_4 does not exist:

a) I_3 exists, and we utilize Y_i' ($i = 1,\ldots K_1+K_2$) with the two elements $d_{g_1}(C_{K_1})$ and d_{g_2}, or

b) I_3 does not exist, and we eliminate the preceding measurement.

If I_4 exists, we utilize $C(K_2)$ and continue.

Figure 2A.

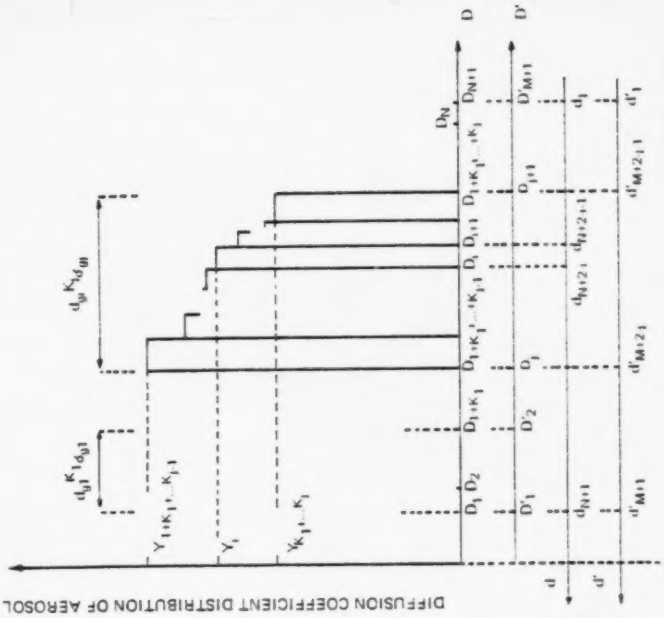

Figure 1A.

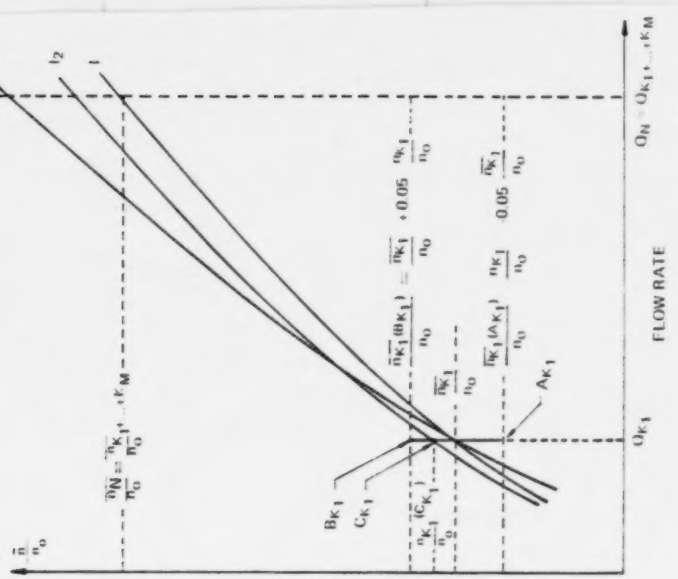

Figure 4A.

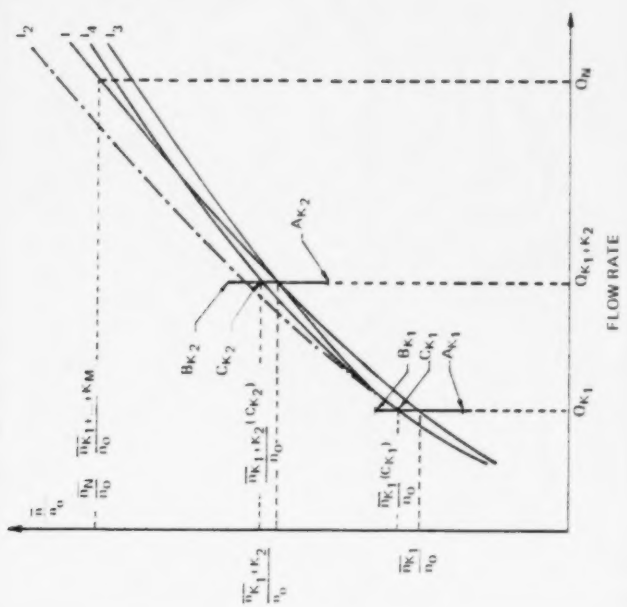

Figure 3A.

```
LEVEL 21.7 ( JAN 73 )                          OS/360  FORTRAN H

          COMPILER OPTIONS - NAME=  MAIN,OPT=02,LINECNT=60,SIZE=0000K,
                             SOURCE,EBCDIC,NOLIST,NODECK,LOAD,MAP,NOEDIT,ID,NOXREF
  ISN 0002              DIMENSION E(25),B(25),Q(25),D(25),SGING1(25,50),Y4(25),H4(25),
                       1BM(25,25),DIA(25),DIAG(25),X1(25,50),P(25,50),DIA1(25),BC(50),
                       2HA(25),K1(25),DGIN1(25,50),HB(25),K2(25),QA(25),HC(25),PAS(50),
                       3BE(50),JK(25),Y1(25,50),Y2(25,25),H(25,50),H2(25,25)
  ISN 0003              COMMON /UN/QA,H2,K2,HB/DEUX/DIA,DIA1,Y2
  ISN 0004              READ(5,301) NM1,NM2,NM3,V,W,YA,UV,DIA1(1),LA,N4
  ISN 0005      301     FORMAT (3I2,2F6.2,F6.1,F6.3,F9.6,2I4)
  ISN 0006              N5=N4+1
  ISN 0007              READ (5,302) (QA(I),I=1,N4)
  ISN 0008      302     FORMAT (16F5.2)
  ISN 0009              READ (5,303)(K1(IA),IA=1,LA)
  ISN 0010      303     FORMAT (20I4)
  ISN 0011              READ (5,304) (HA(I),I=1,LA)
  ISN 0012      304     FORMAT (10F8.5)
  ISN 0013              DO 603 J=1,LA
  ISN 0014              HC(J)=HA(J)
  ISN 0015      603     K2(J)=K1(J)
  ISN 0016              LD=LA
  ISN 0017              A=3.77*V*W*YA/UV
  ISN 0018              DO 101 I=1,N4
  ISN 0019              Q(I)=QA(I)*100./6.
  ISN 0020              E(I)=A/Q(I)
  ISN 0021              D(I+1)=-(ALOG(0.01/0.909))/E(I)
  ISN 0022      101     CONTINUE
  ISN 0023              AE=(1.3804*293.*1.E-07)/(3.*3.1416*18.5)
  ISN 0024              AF=1.246*0.653*0.2
  ISN 0025              AG=0.42*0.653*0.2
  ISN 0026              AH=0.87/(0.653*0.2)
  ISN 0027              D(1)=AE/DIA1(1)*(1+AF/DIA1(1)+AG/DIA1(1)*EXP(-AH*DIA1(1)))
                C                     DECOUPAGE EN CLASSES DE DIAMETRES
  ISN 0028              DO 102 I=1,N4
```

Figure 5A. Fortran program.

```
ISN 0029            DELTA=(AE**2.)+4.*D(I+1)*(AF+AG)*AE
ISN 0030            CA=(AE+SQRT(DELTA))/(2.*D(I+1))
ISN 0031            FOG=CA/2.
ISN 0032      27    DIF=(1.+AF/CA+AG/CA*EXP(-AH*CA))*AE/CA
ISN 0033            IF(DIF-D(I+1))22,23,23
ISN 0034      22    CB=CA-FOG
ISN 0035            GO TO 25
ISN 0036      23    CB=CA+FOG
ISN 0037      25    FOG=FOG/2.
ISN 0038            IF(ABS(CA-CB).LT.1E-05) GO TO 26
ISN 0040            CA=CB
ISN 0041            GO TO 27
ISN 0042      26    DIA(I)=CB
ISN 0043      102   CONTINUE
ISN 0044            AP=2.*(1.-0.9999)
ISN 0045            COS=APIERF(AP)
ISN 0046            WRITE(6,210) V,W,YA,UV,COS,DIA1(1),LA
ISN 0047      210   FORMAT (4H  V=F6.2,5H   W=F6.2,6H   YA=F6.1,6H   UV=F6.3,7H   COS=
                   1F5.2,11H   DIA1(1)=F9.6,6H   LA=I4)
ISN 0048            WRITE(6,211) (QA(I),I=1,N4)
ISN 0049      211   FORMAT('0DEBITS',12X,6(9F11.2//8X,F11.2))
ISN 0050            WRITE(6,212) (D(J),J=1,N5)
ISN 0051      212   FORMAT('0COEF DIFF  ',6(10E11.3//12X))
ISN 0052            WRITE(6,213) (DIA(I),I=1,N4)
ISN 0053      213   FORMAT('0DIAMETRES',10X,6(9F11.4//9X,F11.4))
ISN 0054            WRITE (6,214) (HA(I),I=1,LA)
ISN 0055      214   FORMAT('0MESURES  ',5(12F9.5//10X))
ISN 0056            WRITE(6,215) (K1(IA),IA=1,LA)
ISN 0057      215   FORMAT('0,K1= ',30I4///)
ISN 0058            DO 1000 IR=1,N4
ISN 0059            B(IR)=42.86*V*W*YA/(UV*Q(IR))
ISN 0060            DO 100 M=1,N4
ISN 0061            IF (M-IR) 10,10,15
ISN 0062      15    BM(IR,M)=0.
ISN 0063            GO TO 100
```

Figure 5A. (Continued).

```
ISN 0064      10    CL=(EXP(-E(IR)*D(M))-EXP(-E(IR)*D(M+1)))*0.909/E(IR)
ISN 0065            CM=(EXP(-B(IR)*D(M))-EXP(-B(IR)*D(M+1)))*0.053/B(IR)
ISN 0066            BM(IR,M)=(CL+CM)/(D(M+1)-D(M))
ISN 0067      100   CONTINUE
ISN 0068      1000  CONTINUE
ISN 0069            DO 408 IN=1,N4
ISN 0070            DIAG(IN)=ALOG10(DIA(IN))
ISN 0071      408   CONTINUE
ISN 0072            LQ=1
ISN 0073            DO 32 I=1,N4
ISN 0074            IF(I.EQ.K1(LQ)) GO TO 33
ISN 0076            HB(I)=0.
ISN 0077            GO TO 32
ISN 0078      33    HB(I)=HA(LQ)
ISN 0079            LQ=LQ+1
ISN 0080      32    CONTINUE
ISN 0081            CONS=COS
ISN 0082            LB=1
ISN 0083      1710  DO 918 L=LB,LA
ISN 0084            K=1
ISN 0085            INV=K1(L)
ISN 0086            HA(L)=HB(INV)
ISN 0087            IF(L.EQ.1) GO TO 6
ISN 0089            INV1=K1(L-1)
ISN 0090            DIA1(L)=DIA(INV1)
ISN 0091      6     EPS1=0.025*HA(L)
ISN 0092            IF (CONS) 122,120,120
ISN 0093      120   DGIN1(L,K)=DIA1(L)/2.
ISN 0094            PAS(K)=DGIN1(L,K)/2.
ISN 0095            GO TO 1899
ISN 0096      122   DGIN1(L,K)=100.*DIA1(L)
ISN 0097            PAS(K)=(DGIN1(L,K)-DIA1(L))/2.
ISN 0098      1899  DIA1G=ALOG10(DIA1(L))
ISN 0099      899   DGING1=ALOG10(DGIN1(L,K))
ISN 0100            SGING1(L,K)=(DIA1G-DGING1)/CONS
ISN 0101            DO 409 I=1,N4
```

Figure 5A. (Continued).

```
ISN 0102            IF(DIA(I)-DIA1(L))1,3,3
ISN 0103      3     IF(K.NE.1) GO TO 4
ISN 0105            X1(I,K)=X1(I,KM)
ISN 0106            P(I,K)=P(I,KM)
ISN 0107            GO TO 409
ISN 0108      4     P(I,K)=P(I,K-1)
ISN 0109            X1(I,K)=X1(I,K-1)
ISN 0110            GO TO 409
ISN 0111      1     X1(I,K)=(DIAG(I)-DGING1)/SGING1(L,K)
ISN 0112            X=X1(I,K)
ISN 0113            P(I,K)=AFGP(X)
ISN 0114      409   CONTINUE
ISN 0115            Y1(1,K)=1.-P(1,K)
ISN 0116            DO 421 I=2,N4
ISN 0117            Y1(I,K)=P(I-1,K)-P(I,K)
ISN 0118      421   CONTINUE
ISN 0119            DO 420 IR=1,N4
ISN 0120            H(IR,K)=0.
ISN 0121            DO 520 M=1,N4
ISN 0122            H(IR,K)=H(IR,K)+BM(IR,M)*Y1(M,K)
ISN 0123      520   CONTINUE
ISN 0124      420   CONTINUE
ISN 0125            BC(K)=(H(INV,K)-HA(L))/HA(L)
ISN 0126            IF(ABS(BC(K)).LE.1E-03) GO TO 8
ISN 0128      2     IF(ABS((DIA1(L)-DGIN1(L,K))/DIA1(L)).LT.1E-04) GO TO 8
ISN 0130            KN=K+1
ISN 0131            IF(CONS) 132,130,130
ISN 0132      130   IF(DGIN1(L,K).LE.1E-04) GO TO 8
ISN 0134            IF(BC(K))7,8,9
ISN 0135      132   IF(DGIN1(L,K).GE.(150.*DIA1(L))) GO TO 8
ISN 0137            IF(BC(K))9,8,7
ISN 0138      7     DGIN1(L,KN)=DGIN1(L,K)+PAS(K)
ISN 0139            GO TO 21
ISN 0140      9     DGIN1(L,KN)=DGIN1(L,K)-PAS(K)
ISN 0141      21    PAS(KN)=PAS(K)/2.
ISN 0142            K=KN
```

Figure 5A. (Continued).

```
ISN 0143            GO TO 899
ISN 0144      8     KM=K
ISN 0145      11    IF(HB(N4)-H(N4,KM))17,1100,19
ISN 0146      17    IF(EPS1.LT.0.0002*HB(INV)) GO TO 1100
ISN 0148            HA(L)=HA(L)-EPS1
ISN 0149            GO TO 20
ISN 0150      19    IF(EPS1.LT.0.0002*HB(INV)) GO TO 1100
ISN 0152            HA(L)=HA(L)+EPS1
ISN 0153      20    EPS1=EPS1/2.
ISN 0154            WRITE (6,202) DGIN1(L,KM),SGING1(L,KM)
ISN 0155      202   FORMAT(//,15X,2F9.6)
ISN 0156            DO 50 I=1,N4
ISN 0157            H4(I)=H(I,KM)
ISN 0158      50    Y4(I)=Y1(I,KM)
ISN 0159            CALL ECRIT (Y4,H4,N4)
ISN 0160            DO 14 KM=1,K
ISN 0161            BE(KM)=(H(INV,KM)-HA(L))/HA(L)
ISN 0162            IF(ABS(BE(KM)).LE.1E-03) GO TO 12
ISN 0164            IF(BC(KM)*BE(KM)) 31,35,35
ISN 0165      35    BC(KM)=BE(KM)
ISN 0166      14    CONTINUE
ISN 0167            KM=K
ISN 0168      31    BC(KM)=BE(KM)
ISN 0169            K=KM
ISN 0170            GO TO 2
ISN 0171      12    BC(KM)=BE(KM)
ISN 0172            K=KM
ISN 0173            GO TO 11
ISN 0174      1100  BG=ABS((DIA1(L)-DGIN1(L,KM))/DIA1(L))
ISN 0175            IF(BG.LT.1E-04) GO TO 2200
ISN 0177            IF(CONS) 142,140,140
ISN 0178      140   IF(DGIN1(L,KM).LE.1E-04) GO TO 2200
ISN 0180            GO TO 1314
ISN 0181      142   IF(DGIN1(L,KM).GE.(150.*DIA1(L))) GO TO 2200
ISN 0183      1314  CONS=X1(INV,KM)
ISN 0184            JK(L)=KM
```

Figure 5A. (Continued).

```
ISN 0185              DO 160 I=1,N4
ISN 0186              Y2(L,I)=Y1(I,KM)
ISN 0187              H2(L,I)=H(I,KM)
ISN 0188        160   CONTINUE
ISN 0189              WRITE (6,217)
ISN 0190        217   FORMAT ('0AJUSTEMENT'///)
ISN 0191        918   CONTINUE
ISN 0192              GO TO 2300
ISN 0193        2200  IF(L-2) 88,88,89
ISN 0194        89    INV=K1(L-2)
ISN 0195              CONS=X1(INV,KM)
ISN 0196              LB=L-1
ISN 0197              GO TO 90
ISN 0198        88    CONS=COS
ISN 0199              LB=1
ISN 0200        90    LA=LA-1
ISN 0201              DO 2320 MH=LB,LA
ISN 0202              K1(MH)=K1(MH+1)
ISN 0203        2320  CONTINUE
ISN 0204              WRITE (6,218)
ISN 0205        218   FORMAT ('0REJET'///)
ISN 0206              GO TO 1710
ISN 0207        2300  DO 450 L=1,LA
ISN 0208              JP=JK(L)
ISN 0209              WRITE (6,205) K1(L),DGIN1(L,JP),SGING1(L,JP)
ISN 0210        205   FORMAT(////,5X,I4,2F9.6)
ISN 0211              DO 51 I=1,N4
ISN 0212              H4(I)=H2(L,I)
ISN 0213        51    Y4(I)=Y2(L,I)
ISN 0214              CALL ECRIT (Y4,H4,N4)
ISN 0215        450   CONTINUE
ISN 0216              WRITE(6,221)
ISN 0217        221   FORMAT('1',19X,'CLASSES',5X,'POURCENTAGES  MESURES',6X,'MESURES
     ,                1ECARTS'/20X,'DIAMETRES   PARTICULES    RESTITUEES   DONNEES   EN %
                      2')
ISN 0218              WRITE(6,222) DIA1(1)
```

Figure 5A. (Continued).

```
ISN 0219      222   FORMAT(20X,F9.5/)
ISN 0220            SOM=0.
ISN 0221            J=1
ISN 0222            DO 423 I=1,N4
ISN 0223            SOM=SOM+Y4(I)
ISN 0224            BP=100.*Y4(I)
ISN 0225            WRITE(6,224) BP
ISN 0226      224   FORMAT(31X,F6.2)
ISN 0227            IF(I.EQ.K2(J)) GO TO 424
ISN 0229            WRITE(6,223) DIA(I),H4(I)
ISN 0230      223   FORMAT(20X,F9.5,17X,F8.5)
ISN 0231            GO TO 423
ISN 0232      424   BQ=100.*((H4(I)-HC(J))/HC(J))
ISN 0233            WRITE(6,225) DIA(I),H4(I),HC(J),BQ
ISN 0234      225   FORMAT(20X,F9.5,17X,F8.5,5X,F8.5,3X,F6.2)
ISN 0235            J=J+1
ISN 0236      423   CONTINUE
ISN 0237            WRITE (6,220) SOM
ISN 0238      220   FORMAT (////,20X,'SOMME='F7.3)
ISN 0239            IF (NM1.EQ.0) GO TO 503
ISN 0241            CALL HISTO (N4,N5,LA)
ISN 0242      503   IF (NM2.EQ.0) GO TO 501
ISN 0244            CALL COURBE (N4,LA,LD)
ISN 0245      501   IF (NM3.EQ.0) GO TO 502
ISN 0247            CALL PRECUM (N4,LA)
ISN 0248      502   STOP
ISN 0249            END
```

Figure 5A. (Continued).

```
LEVEL 21.7 ( JAN 73 )                    OS/360  FORTRAN H                    DATE  79

          COMPILER OPTIONS - NAME=  MAIN,OPT=02,LINECNT=60,SIZE=0000K,
                             SOURCE,EBCDIC,NOLIST,NODECK,LOAD,MAP,NOEDIT,ID,NOXREF
  ISN 0002              SUBROUTINE ECRIT (A,B,N)
  ISN 0003              DIMENSION A(N),B(N)
  ISN 0004              WRITE (6,1) A
  ISN 0005       1      FORMAT(/,(10X,12F9.5))
  ISN 0006              WRITE (6,2) B
  ISN 0007       2      FORMAT(/,(15X,12F9.5))
  ISN 0008              RETURN
  ISN 0009              END
```

Figure 5A. (Continued).

```
LEVEL 21.7 ( JAN 73 )                    OS/360  FORTRAN H                    DATE  79

          COMPILER OPTIONS - NAME=  MAIN,OPT=02,LINECNT=60,SIZE=0000K,
                             SOURCE,EBCDIC,NOLIST,NODECK,LOAD,MAP,NOEDIT,ID,NOXREF
 ISN 0002              SUBROUTINE COURBE (N4,LA,LD)
 ISN 0003              DIMENSION TR(200)
 ISN 0004              COMMON/UN/QA(25),H2(25,25),K2(25),HB(25)
 ISN 0005              CALL TADEB(25,33.,25.)
 ISN 0006              CALL TAAXE(0,2.,2.,1.,0.)
 ISN 0007              CALL TBXECH(1,30.,0.,QA(N4),0.5,0.5,6,6HDEBITS)
 ISN 0008              CALL TBXECH(2,20.,0.,H2(LA,N4),0.5,0.5,7,7HMESURES)
 ISN 0009              CALL TATXT(0,1.,21.,0.5,0.,41,'COURBES EXPERIMENTALE(0) ET RECALCU
                      1LEE(1)',0)
 ISN 0010              CALL TBREPR(3.,3.,0.5,1,'1',0)
 ISN 0011              DO 601 I=1,N4
 ISN 0012      601     CALL TBLS2 ((N4-4+I)/(N4-2),QA(I),H2(LA,I),TR,200)
 ISN 0013              CALL TBRFIN(0)
 ISN 0014              CALL TBREPR(3.,3.,0.5,1,'0',0)
 ISN 0015              DO 602 J=1,LD
 ISN 0016              LM=K2(J)
 ISN 0017      602     CALL TBLS2((LD-4+J)/(LD-2),QA(LM),HB(LM),TR,200)
 ISN 0018              CALL TBRFIN(0)
 ISN 0019              CALL TAFIN
 ISN 0020              RETURN
 ISN 0021              END
```

Figure 5A. (Continued).

```
LEVEL 21.7 ( JAN 73 )                OS/360  FORTRAN H                DATE  79.347/09.45.26

          COMPILER OPTIONS - NAME= MAIN,OPT=02,LINECNT=60,SIZE=0000K,
                             SOURCE,EBCDIC,NOLIST,NODECK,LOAD,MAP,NOEDIT,ID,NOXREF
 ISN 0002                    SUBROUTINE FRECUM (N4,LA)
 ISN 0003                    DIMENSION PC(25),B(13),TXT(13)
 ISN 0004                    COMMON/DEUX/D(25),DIA1(25),C(25,25)
 ISN 0005                    DATA B/3.,6.8,12.,14.3,15.8,17.2,18.4,19.7,21.1,22.6,24.9,30.1,
                            133.9/
 ISN 0006                    DATA TXT/4H99.9,4H99  ,4H90  ,4H80  ,4H70  ,4H60  ,4H50  ,4H40  ,4
                            1H30  ,4H20  ,4H10  ,4H1.  ,4H0.1 /
 ISN 0007                    PD=0.
 ISN 0008                    DO 52 I=1,N4
 ISN 0009                    PD=PD+C(LA,I)
 ISN 0010                    PA=1.-2.*(ABS(0.5-PD))
 ISN 0011                    PB=AFIERF(PA)
 ISN 0012                    IF(PD.GE.0.5) GO TO 53
 ISN 0014                    PC(I)=15.+PB*5.
 ISN 0015                    GO TO 52
 ISN 0016           53       PC(I)=15.-PB*5.
 ISN 0017           52       CONTINUE
 ISN 0018                    CALL TADEB(25,35.,35.)
 ISN 0019                    DO 100 I=1,13
 ISN 0020                    CALL TATXT(0,1.,B(I),0.3,0.,4,TXT(I),0)
 ISN 0021                    CALL TADEP(0,3.5,B(I))
 ISN 0022           100      CALL TADEP(5,0.5,0.)
 ISN 0023                    CALL TADEP(5,0.,-30.9)
 ISN 0024                    CALL TAAXE(0,4.,3.,1.,0.)
 ISN 0025                    CALL TBXECH(-1,30.,D(N4),D(1),0.5,0.4,9,9HDIAMETRES)
 ISN 0026                    CALL TADEP(2,D(1),PC(1))
 ISN 0027                    DO 56 I=2,N4
 ISN 0028           56       CALL TADEP(3,D(I),PC(I))
 ISN 0029                    CALL TAFIN
 ISN 0030                    RETURN
 ISN 0031                    END
```

Figure 5A. (Continued).

```
LEVEL 21.7 ( JAN 73 )                                    OS/360  FORTRAN H

        COMPILER OPTIONS - NAME=  MAIN,OPT=02,LINECNT=60,SIZE=0000K,
                           SOURCE,EBCDIC,NOLIST,NODECK,LOAD,MAP,NOEDIT,ID,NOXREF
ISN 0002                SUBROUTINE HISTO (N4,N5,LA)
ISN 0003                COMMON/DEUX/DIA(25),DIA1(25),Y2(25,25)
ISN 0004                DIMENSION DIX(25),Y3(25)
ISN 0005                DO 440 I=1,N4
ISN 0006      440       DIX(I)=DIA(N5-I)
ISN 0007                DIX(N5)=DIA1(1)
ISN 0008                DO 506 I=1,N4
ISN 0009      506       Y3(I)=Y2(LA,N5-I)/ABS(DIX(I)-DIX(I+1))
ISN 0010                AM=0.
ISN 0011                DO 510 I=1,N4
ISN 0012      510       AM=AMAX1(AM,Y3(I))
ISN 0013                DO 502 I=1,N4
ISN 0014                IF(Y3(I).GE.(AM/50.)) GO TO 503
ISN 0016      502       CONTINUE
ISN 0017      503       IF(I.EQ.1) GO TO 505
ISN 0019                N4=N4-I+1
ISN 0020                N5=N5-I+1
ISN 0021                DO 504 J=1,N4
ISN 0022                Y3(J)=Y3(J+I-1)
ISN 0023                DIX(J)=DIX(J+I-1)
ISN 0024      504       CONTINUE
ISN 0025                DIX(N5)=DIX(N5+1)
ISN 0026      505       CALL TADEB (25,30.,33.)
ISN 0027                CALL TAAXE (0,4.,2.,1.,0.)
ISN 0028                CALL TBXECH(1,24.,DIX(1),DIX(N5),0.5,0.5,9,9HDIAMETRES)
ISN 0029                CALL TBXECH(2,30.,0.,AM,0.5,0.5,11,11HHISTOGRAMME)
ISN 0030                CALL TADEP (2,DIX(1),0.)
ISN 0031                DO 507 I=1,N4
ISN 0032                CALL TADEP (3,DIX(I),Y3(I))
ISN 0033                CALL TADEP (3,DIX(I+1),Y3(I))
ISN 0034                IF(I.EQ.N4) GO TO 509
```

Figure 5A. (Continued).

```
ISN 0036              IF (Y3(I).GE.Y3(I+1)) GO TO 508
ISN 0038              CALL TADEP (2,DIX(I+1),0.)
ISN 0039              GO TO 507
ISN 0040        508   CALL TADEP (3,DIX(I+1),Y3(I+1))
ISN 0041              CALL TADEP (2,DIX(I+1),0.)
ISN 0042        507   CONTINUE
ISN 0043        509   CALL TADEP (3,DIX(N5),0.)
ISN 0044              CALL TAFIN
ISN 0045              RETURN
ISN 0046              END
```

Figure 5A. (Continued).

APPENDIX B

INTRODUCTION OF COUNTING LOSSES IN THE MAIGNE METHOD

THE $\bar{n}_i/n_o$ RATIO

Let f(D) be the size distribution function of the particles under study; f(D) depends on the diffusion coefficient of the particles, and the diffusion coefficient depends only on the corresponding particle diameter d. The intervals are defined arbitrarily.

$$D_1D_2,\ D_2D_3 \cdots D_iD_{i+1} \cdots\cdots D_{N-1}D_{Ni}D_ND_{N+1}$$

where $D_{i+1} > D_i$ $(i = 1,N)$

For $1 < i < N$, we assign to D_{i+1} corresponding values, experimentally determined, of the flow rate Q_i through the battery. For the paired values D_{i+1}, Q_i, the function

$$\bar{n}_i/n_o = 0.01$$

where $\bar{n}_i$ = mean concentration of the particles of all dimensions transmitted by the diffusion battery

n_o = the upstream particle concentration

the $\bar{n}_i$ and n_o quantities being measured by a condensation nuclei counter (CNC). Neglecting counting losses of the CNC, we can write

$$\frac{\bar{n}_i}{n_o} = \frac{\int_{D_i}^{D_{i+1}} f(D)\ \rho(D,Q_i)dD}{n_o} = \frac{\int_{D_i}^{D_{i+1}} f(D)\ \rho(D,Q_i)dD}{\int_0^{\infty} f(D)\ dD} \qquad \text{(B-1)}$$

Preceding page blank

The term, $\rho(D,Q_i)$, representing the transmission function of the battery, depends on D_iQ_i and the characteristics of the battery, but is independent of f.

The approximation permitting a determination for the function f consists of taking sufficiently small segments for f(D) to remain constant along the interval $D_i\ D_{i+1}$. Let Y_i be the constant value of f(D) along every one of these segments. Let

$$X_{ij} = \int_{D_j}^{D_{j+1}} \rho(D_iQ_i)dD \qquad \text{(B-2)}$$

We shall write

$$\frac{\overline{n_i}}{n_o} = \frac{1}{n_o} \sum_{j=1}^{j=1} X_{ij}Y_j \qquad \text{(B-3)}$$

REAL SIZE DISTRIBUTION

Counting losses of the CNC increase as d decreases. Let N_c be the number of particles indicated and N_a the real number of particles. The ratio N_c/N_a can be defined as:

$$\frac{N_c}{N_a} = \alpha\ (D) = \beta\ (d)$$

where α and β are functions of D and d, determined by successive, distinct, experimental points. Expression (1), inclusive of counting losses, has the real value

$$\frac{n_i}{n_o} = \frac{\int_{D_i}^{D_{i+1}} \alpha(D)\ f(D)\ \rho(D,Q_i)\ dD}{\int_0^{\infty} \alpha(D)\ f(D)\ dD} \qquad \text{(B-4)}$$

This means that the corresponding size distribution function, f(D), is incorrect, and that the real size distribution function f(D) is given by

$$f'(D) = \alpha(D)\, f(D) = \beta(d)\, \Psi(d) \qquad \text{(B-5)}$$

where d = the diameter of particles whose diffusion coefficient is D

The real size distribution of the aerosol will be given by

$$f(D) = [\alpha(D)]^{-1} f'(D) = [\beta(d)]^{-1}\, \Psi(d) \qquad \text{(B-6)}$$

CORRECTING VALUES IN ASSOCIATED FUNCTIONS

We have written

$$\frac{n_i}{n_o} = \frac{1}{n_o} \sum_{j=1}^{j=i} X_{ij} Y_{ij} = \frac{\sum_{j=1}^{j=i} X_{ij} Y_j}{\sum_{j=1}^{j=N} Y_i (D_{j+1} - D_j)} \qquad \text{(B-7)}$$

The numerical method of Maigne has been used tocalculate X_{ij}, and Y_j are the different values assumed constant for the f(D) function along each interval of the diffusion coefficient $D_j D_{j+1}$. If we assume that along each interval $D_j D_{j+1}$, the coefficient characterizing the counting losses has a constant value $\alpha(D_j) = \beta(d_j)$, where D_j and d_j represent the mean values of D and d, respectively, along intervals $D_j D_{j+1}$ or $d_j d_{j-1}$, Relation (B-7) gives:

$$\frac{\overline{n_i}}{n_o} = \frac{\sum_{j=1}^{j=i} X_{ij}\, \alpha(D_j) Y_j^*}{\sum_{j=1}^{j=N} (D_j)\, Y_j^* (D_{j+1} - D_j)} \qquad \text{(B-8)}$$

The percentage of particles along the intervals $D_j D_{j+1}$, without regard for counting losses, previously represented by:

$$Y_j' = \frac{Y_j\ (D_{j+1} - D_j)}{\sum_{j=1}^{N} Y_j\ (D_{j+1} - D_j)} \qquad \text{(B-9)}$$

is now represented by

$$Y_j'^* = \frac{Y_j^*\ (D_{j+1} - D_j)}{\sum_{j=1}^{N} Y_j^*\ (D_{j+1} - D_j)} \qquad \text{(B-10)}$$

Therefore, the following relation may be written

$$Y_j'^* = \frac{(\alpha_j)^{-1}\ Y_j'\ (D_{j+1} - D_j)}{\sum_{j=1}^{N} (\alpha_j)^{-1}\ Y_j'\ (D_{j+1} - D_j)} \qquad \text{(B-11)}$$

If, for a given size distribution, we are interested in the function $(\Delta N/\Delta d)_j$, ΔN_j is the number of particles along the interval $D_j D_{j+1}$; or

$$\Delta d = d_j - d_{j+1} \qquad \text{(B-12)}$$

If we do not consider the counting losses, we have

$$\left(\frac{\Delta N}{\Delta d}\right)_j = \frac{Y_j}{\Delta d_j} \qquad \text{(B-13)}$$

If we introduce counting losses,

$$\left(\frac{\Delta N}{\Delta d}\right)^* = \frac{Y_j^*}{\Delta d_j} \qquad \text{(B-14)}$$

and, according to Equation 14, we may write

$$\left(\frac{\Delta N}{\Delta d}\right)_j = (\alpha_j)^{-1} \left(\frac{\Delta N}{\Delta d_j}\right) \qquad \text{(B-15)}$$

METHOD ERROR

The experimental curve representing Y as a function of D or d is, on the whole, a set of segments. The counting losses are also measured for discontinuous values of d, and consequently of D.

If we wish to calculate more exactly, we must establish an analytical function that considers counting loss and particle diameter, and we must modify the integration method (Twomey, for example). This is impossible in actual experimental conditions.

On the other hand, an empirical equation representing a continuous correction based on discontinuous measurements can introduce additional errors, because the empirical relation cannot perfectly represent the correction.

For the counter we used, we obtained a linear relation for $d < 0.06\ \mu m$, but a discontinuity exists for greater values.

Finally, we do not disregard methods other than the one of Maigne. It seems preferable for this time to adopt a mean correction in the interval $D_i\ D_{i+1}$, which is the corresponding experimental value of α or β.

BEGIN FIRST LINE OF TEXT HERE
TYPING GUIDE SHEET
CENTER OF PAGE
TOP OF IMAGE AREA
DROPPED HEAD BEGIN SECTIONS HERE
6-1/2"
9-1/8"
BEGIN LAST LINE OF TEXT
BOTTOM OF IMAGE AREA OUTSIDE DIMENSION FOR TABLES AND ILLUSTRATIONS
3/8"
PAGE NUMBER
EPA-287 (C16.1)
(4-76)

REFERENCE

Twomey, S. J. Franklin Inst., 215:121, 1963.